On shear viscosity and the Reynolds number of MHD turbulence in collisionless magnetized plasmas: Coulomb collisions, Landau damping, and Bohm diffusion

Joseph E. Borovsky and S. Peter Gary

Los Alamos National Laboratory, Los Alamos, New Mexico 87545 USA

For a collisionless plasma, the magnetic field $\underline{B}$ enables fluid-like behavior in the directions perpendicular to B; however fluid behavior along $\underline{B}$ may fail. The magnetic field also introduces an Alfven-wave nature to flows perpendicular to $\underline{B}$. All Alfven waves are subject to Landau damping, which introduces a flow dissipation (viscosity) in collisionless plasmas. For three magnetized plasmas (the solar wind, the Earth's magnetosheath, and the Earth's plasma sheet) shear viscosity by Landau damping, Bohm diffusion, and by Coulomb collisions are investigated. For MHD (magnetohydrodynamic) turbulence in those three plasmas integral-scale Reynolds numbers are estimated, Kolmogorov dissipation scales are calculated, and Reynolds-number scaling is discussed. Strongly anisotropic Kolmogorov $k^{-5/3}$ and mildly anisotropic Kraichnan $k^{-3/2}$ turbulences are both considered and the effect of the degree of wavevector anisotropy on quantities such as Reynolds numbers and spectral-transfer rates are calculated. For all three plasmas, Braginskii shear viscosity is much weaker than shear viscosity due to Landau damping which is somewhat weaker than Bohm diffusion.

I. INTRODUCTION: REYNOLDS NUMBERS, COLLISIONLESS PLASMAS, AND VISCOSITY

This manuscript addresses the dissipation of turbulent fluctuations in magnetized, collisionless plasmas in terms of shear viscosity. This section begins with a discussion of these topics in inhomogeneous Navier-Stokes fluids, and then provides a discussion of how viscosity and Reynolds numbers must be treated differently in magnetized, collisionless plasmas.

There are several ways to define a Reynolds number. A straightforward generalized definition (cf. eq. (1.4.6) of Tennekes and Lumley[1]) is the ratio of a dissipation timescale τ_{diss} to a convection timescale τ_{conv} for a flow structure

$$R = \tau_{diss}/\tau_{conv} \qquad . \tag{1}$$

For a size L and flow velocity U, the convection (dynamical) timescale is $\tau_{conv} = L/U$. For Newtonian fluids with kinematic viscosity ν the dissipation (diffusion) timescale is $\tau_{diss} = L^2/\nu_{kin}$. Using these two relations, expression (1) becomes

$$R = UL/\nu \quad , \tag{2}$$

the original definition of the Reynolds number[2]. The interpretation of what the Reynolds number R means depends on what is used for u and for L.

Commonly, in evaluating expression (2) the velocity U is taken to be a bulk flow velocity and L is taken to be the scalesize of gradients in the bulk flow. In this case it is useful to refer to R as a "flow Reynolds number". As a rule, the flow of a Newtonian fluid is turbulent when the flow Reynolds number is sufficiently high (cf. Refs. 2-5, Ch. 19 of Tritton[6], Sect. XVI.a of Schlichting[7]).

Another way to use equation (2) to define a Reynolds number in a flow that is turbulent is to take U to be the velocity amplitude u_o of the fluctuations in the flow at the large-eddy scalesize, L to be the typical scalesize of a large eddy L_o (the integral scale), and ν to be the kinematic viscosity of the fluid. In this case

$$R_{turb} = u_o L_o / \nu \tag{3}$$

describes the dynamics of a large eddy in the turbulence and R_{turb} is in this case called the "turbulence Reynolds number" or "integral-scale Reynolds number" (cf. Ref. 8). Expression (3) is consistent with (cf. expression (1))

$$R_{turb} = \tau_{diss}/\tau_{eddy-o} \qquad . \tag{4}$$

where $\tau_{eddy-o} = L_o/u_o$ is the eddy turnover timescale of the largest eddies of the turbulence and τ_{diss} is the viscous dissipation time of a large eddy, which is $\tau_{diss} = L_o^2/\nu$ for viscous dissipation.

In this report expression (4) for the turbulence Reynolds number will be generalized to the expression

$$R_{turb} \ = \ \tau_{diss}/\tau_{spectral-o} \qquad , \qquad (5)$$

where $\tau_{spectral-o}$ is the spectral transfer time at the large eddy scalesize and τ_{diss} is the dissipation time of a large eddy. For Navier-Stokes turbulence $\tau_{spectral} = \tau_{eddy}$, the rate of spectral transfer of energy from large eddies to small eddies is proportional to the local eddy turnover time (Ref. 8, Sect. 6.7.1 of Ref. 9). For MHD (magnetohydrodynamic) turbulence , the expression used for $\tau_{spectral}$ will depend on whether Kolmogorov $k^{-5/3}$ turbulence or Kraichnan $k^{-3/2}$ turbulence is being considered. When Kolmogorov turbulence is considered, $\tau_{spectral} = \tau_{eddy}$ and expression (3) is obtained for R_{turb}. The expression for R_{turb} for Kraichnan turbulence will be derived in Section II.A.

In Navier-Stokes turbulence the turbulence Reynolds number must be somewhat above unity, but need not be extremely large[10-12]. Among other things, the turbulence Reynolds number in Navier-Stokes fluids provides information about the range of scalesizes of the fluctuations in the turbulence (e.g. pg. 21-22 of Ref. 1).

For concepts such as viscosity and Reynolds number a collisionless plasma presents some difficulties. A collisionless plasma is a plasma in which (1) particle-collision timescales (momentum-exchange timescales) are much larger than any dynamical timescale (i.e., ion and electron gyroperiods, ion and electron plasma periods, wave periods, and flow dynamical timescales) and (2) particle mean free paths are much larger than characteristic scalesizes (i.e. gradient scales, gyroradii, skin depths, wavelengths, and even system sizes).

A collisionless magnetized plasma has several important differences from a Navier-Stokes fluid. The magnetized plasma has fluid-like properties owing to the fact that the particles of the plasma are constrained to orbit the magnetic-field lines[13,14]; hence the plasma "holds together", at least in the direction perpendicular to $\underline{B}$. The magnetic field introduces an anisotropy to the medium. The field also introduces waves to the medium: any flow structure perpendicular to $\underline{B}$ will propagate along the magnetic field ducted as an Alfven wave (Sect. 3.6 of Ref. 15, Refs. 16-18).

Viscosity is a relatively simple concept in an isotropic Newtonian fluid. Here the viscosity is the single scalar constant of proportionality relating the stress tensor to the rate-of-strain tensor[19,20]. In this case the shear viscosity that acts on shearing motions is directly related to the bulk viscosity (second viscosity) that acts on compressive motions (cf. Sect. 5.6 of Ref. 6 and Sect. 6.3 of Ref. 21).

For a "collisionless" magnetized plasma, there is no simple definition of viscosity. Owing to the anisotropy of a magnetized plasma the coefficients relating the terms of the stress tensor to the various terms of the rate-of-strain tensor can be quite complicated, even for classical processes (cf. Ref. 22 and Sect. 18.44 of Ref. 23). In this paper, only the coefficients pertaining to shear motion strictly perpendicular to $\underline{B}$ will be of interest (the Type-II motion of Kaufman[24]) and these coefficients will be called the coefficients of shear viscosity of the plasma. These shear-viscosity coefficients will be used in this paper to calculate dissipation timescales for shear motions and to estimate turbulence Reynolds numbers for MHD turbulence in collisionless magnetized plasmas. (In the Appendix, it is argued that the flows and shears of MHD turbulence are predominantly perpendicular to the magnetic field of the plasma.) One could envision inserting these shear-viscosity coefficients into the MHD equations to describe the effects of Vlasov processes ongoing in large-scale collisionless plasmas.

Coulomb scattering can supply some electrical resistivity (conductivity) and viscosity[22,24-26] that can meaningfully act on structures perpendicular to $\underline{B}$ but the Coulomb-scattering mean free paths in the parallel direction are in general larger than the scalesizes of interest, making parallel viscosities that act on parallel-to-$\underline{B}$ motions ill defined (cf. Montgomery[28]). Note, in the direction parallel to $\underline{B}$ not only is the viscosity ill defined, but the plasma behavior may not even be fluid like. Thus MHD might not provide a meaningful description of a collisionless plasma such as the solar wind. For MHD to be formally valid along $\underline{B}$, the collisional mean free path must be smaller than any scalelength of interest (e.g. Sect. 2.0 of Piddington[29] or eq. (3-88) of Boyd and Sanderson[30]). General warnings about using MHD for collisionless plasmas have appeared in textbooks (cf. Sect. 13.0 of Montgomery and Tidman[31] or Sect. 6-4 of Cowling[32]) and warnings specifically about MHD use for the solar wind[33,34] and for the plasmas of the magnetosphere[35] have appeared in the literature. In fact, the solar-wind plasma fails tests of fluid behavior in the direction parallel to $\underline{B}$. Three such failures are the following. (1) The ballistic-particle behavior observed when the collisionless solar-wind plasma and the

collisionless magnetospheric plasma are suddenly joined by magnetic-field-line reconnection[36,37]; fluid behavior would produce a mixing of momentum, i.e. coupling of the two reconnected plasmas, rather than the free interpenetration that is seen. (2) The inability to form a stationary bow shock when the shock normal is parallel to the ambient magnetic field[38-41]. (3) The strictly kinetic dynamics of the solar-wind plasma filling-in the wake of the moon[42,43]. Other collisionless plasmas fail tests of fluid behavior in the parallel-to-$\underline{B}$ direction: colliding laboratory plasmas fail to couple their momenta[44-47] and the plasmas outflowing from the northern and southern ionospheres fail to couple their momenta when they collide in the magnetosphere[48,49]. Collisionless plasma also exhibit the extremely non-fluid phenomena of pseudowaves[50,51] and plasma echoes[52,53], wherein momentum is transported at arbitrary velocities via ballistic particles rather than being shared in a fluid manner.

Three magnetized collisionless plasmas that contain MHD turbulence are the solar wind, the Earth's magnetosheath (the shocked solar wind), and the Earth's plasma sheet. These three plasmas are depicted in Figure 1 and their plasma properties are listed in Table I. The solar wind is a well-known laboratory for MHD turbulence[54-58]. Considerably less work has been done on the MHD turbulence in the high-β plasma sheet[59-63] and on the MHD turbulence of the Earth's magnetosheath[60,64-67]. In all three of these plasmas, there are mean magnetic fields with spatial scales much larger than the correlation lengths of the turbulence in the plasmas. In Table 3 of Borovsky and Funsten[60] the amplitude of the MHD turbulence in these three magnetized plasmas is explored: for all three plasmas $\delta B/B_o \sim 0.5$, meaning that the turbulence in all three cases is strong enough to locally distort the mean fields. Note that there are contradictions (cf. Sects. 5.3.2 and 5.3.3 of Ref. 68) associated with the standard practices of applying Kolmogorov and Kraichnan descriptions of MHD turbulence to the turbulence in a magnetized plasma (such as the solar wind, the magnetosheath, or the plasma sheet). Those contradictions arise from the fact that the Kolmogorov and Kraichnan spectra are derived from dimensional analysis, and that the presence of a mean magnetic field introduces anisotropies to the spectrum of turbulence wavevectors, which prevent the use of dimensional analysis for spectra. These contradictions are not addressed in this paper. Similarly, whether the wavevector spectrum of MHD turbulence in a plasma with a mean magnetic field is isotropic[69,70] or anisotropic[71,72] will not be settled here. In the sections to follow, a factor a describing the degree of anisotropy will be explicitly carried

along in the calculations: the values of this a factor for the turbulences in the plasmas of the heliosphere are as yet unknown. And further, it has yet to be settled which of the two spectral models (Kolmogorov or Kraichnan) is more appropriate for the turbulence in the magnetized plasmas of the heliosphere (cf. Refs. 73-75 versus Refs. 76-78). Therefore, in this paper both spectral phenomenologies (Kolmogorov and Kraichnan) will be separately used for calculations of the Reynolds numbers of the magnetized turbulences in the heliospheric plasmas.

Determining the viscosity of a collisionless magnetized plasma is problematic, not only because of the anisotropy of the plasma but because of the lack of understanding about dissipation mechanisms. In Table II a number of mechanisms that can produce dissipation (diffusion, damping) of MHD-scale fluctuations in a "collisionless" magnetized plasma are listed. In the table the scalesizes over which each mechanism acts is noted. Some mechanisms act at all spatial scales so their dissipation can lead into a Reynolds-number concept. Some mechanisms in Table II only act at the smallest scales (r_{gi}, c/ω_{pi}) where MHD breaks down; these mechanisms can produce a dissipation of the turbulence at the smallest scales of the turbulence (like a hyperviscosity) but do not lead to a Reynolds number. Note that MHD eddy viscosity[79-81] is not included in Table II: eddy viscosity acts as a viscosity on the large-scale flow but does not act as a viscosity on the turbulent fluctuations.

Three of these mechanisms for dissipation in Table II will be explored in this report: Coulomb scattering, Landau damping, and Bohm diffusion. Simple expressions for the shear viscosities will be obtained, written in terms of a spatial scale squared divided by a timescale (cf. eq. (765) of Jeans[82] or Sect. 6.2 of Chapman and Cowling[23]). For these three mechanisms the turbulence Reynolds numbers will be estimated in Sections III-V for the turbulence in the solar wind, the Earth's magnetosheath, and the Earth's plasma sheet. In the calculations, assumptions about the nature of the turbulence cascade must be made. In MHD turbulence there are two major types of turbulence cascades[83-86]: the Kolmogorov $k^{-5/3}$ turbulence and the Kraichnan $k^{-3/2}$ turbulence. Both cascades will be analyzed. In calculating the dissipation of MHD turbulence fluctuations by Landau damping, an assumption about the wavevector anisotropy of the turbulence with respect to the magnetic field must be made and that assumption must be consistent with the type of turbulence cascade: when Kolmogorov $k^{-5/3}$ turbulence is explored the wavevectors of the turbulent fluctuations will be restricted to the reduced-MHD regime below the critical-balance curve will be assumed (strong anisotropy) and when Kraichnan $k^{-3/2}$

turbulence is explored only a mild anisotropy of the turbulence will be assumed. The assumptions made about the wavevector spectra will necessarily make the calculations of the integral-scale Reynolds numbers approximate.

This report is organized as follows. The spectral-transfer rates and anisotropy of Kolmogorov $k^{-5/3}$ and Kraichnan $k^{-3/2}$ MHD turbulences are discussed in Section II. Dissipation of MHD fluctuations by Coulomb scattering is investigated in Section III, dissipation of MHD fluctuations by Landau damping is investigated in Section IV, and dissipation of MHD fluctuations by Bohm diffusion is investigated in Section V. For these three mechanisms the turbulence Reynolds numbers will be estimated for the turbulence in three familiar heliospheric plasmas: the solar wind, the Earth's magnetosheath, and the Earth's plasma sheet. In Section VI the ratios of characteristic scale sizes in MHD turbulence in collisionless plasma is explored in relation to the turbulence Reynolds numbers calculated with various types of viscous processes. In the three subsections of Section VII turbulence in the solar wind, the magnetosheath, and the plasma sheet is discussed. The report is summarized in Section VIII. In the Appendix arguments are presented that the velocity fluctuations in the MHD turbulence of the heliospheric plasmas are predominantly directed perpendicular to the magnetic field of the plasmas.

II. KOLMOGOROV AND KRAICHNAN TURBULENCES

In MHD turbulence there are two major types of turbulence cascades (e.g. Refs. 83-86): the Kolmogorov $k^{-5/3}$ turbulence (Ref. 8) and the Kraichnan $k^{-3/2}$ turbulence (Refs. 87 and 88). Kolmogorov turbulence was developed to describe the cascade of velocity-fluctuation energy in isotropic Navier-Stokes fluids[8]. Nevertheless, it has become one of two formalisms which are often applied to MHD turbulence in collisionless, magnetized, anisotropic plasmas[57,76,89]. The other popular formalism is the Kraichnan description of turbulence, which specifically considers the presence of a magnetic field in the plasma.

Turbulence transfers energy from large-scale fluctuations to smaller-scale fluctuations via eddy-eddy interactions. In Kolmogorov turbulence the spectral transfer of energy proceeds at the local eddy turnover time τ_{eddy}, or some fixed fraction thereof. In Kraichnan turbulence the eddy-eddy interactions are weakened by the "Alfven effect" and the spectral transfer of energy proceeds at a slower rate τ_{weak}. Transfer at the local eddy turnover time produces an omnidirectional energy spectrum that varies as $k^{-5/3}$; transfer at the weakened rate produces an energy spectrum that varies as $k^{-3/2}$.

There are other differences between the two types of turbulence besides the slight difference in the spectral index. Two other differences are noted in the following two paragraphs: one difference deals with the wavevector anisotropy of the turbulence and the other difference deals with the operation of dissipation on the turbulence.

First, the wavevector anisotropy of the turbulence must be consistent with the presence or absence of the Alfven effect. The sketch of the solar-wind in $k_\perp$-$k_\parallel$ space in Figure 2 will aid the discussion. To avoid the Alfven effect (Kolmogorov turbulence), the wavevectors of the turbulence must be nearly perpendicular to the ambient magnetic field of the plasma. That is, the turbulence must be in the reduced-MHD regime[90-92] on or below the critical-balance curve at the boundary of the reduced-MHD regime[93-95]. For the solar wind, this restricts the wavevectors of the MHD turbulence to within 5º of the perpendicular-to-$\underline{B}$ direction (see bottom panel of Figure 2). This Kolmogorov turbulence must have a strong wavevector anisotropy. Since most of $k_\perp$-$k_\parallel$ space is outside of the reduced-MHD regime (see bottom panel Figure 2) quasi-isotropic turbulence will heavily suffer the Alfven effect. Hence, turbulence with only a mild wavevector anisotropy will be Kraichnan turbulence. The degree of wavevector anisotropy of the MHD turbulence in the various heliospheric plasmas is as yet unknown. In calculating the shear

viscosities, Reynolds numbers, etc. of these turbulences, the degree wavevector anisotropy will be parameterized with a factor a defined in Section II.A and that unknown factor a will be carried throughout the manuscript.

Second, the slower rate of spectral transfer in Kraichnan turbulence means that dissipative effects have more time to act on the turbulent fluctuations than they do in Kolmogorov turbulence. This can result in substantially different dissipation scales for the two types of turbulence (the dissipation scale being the scalesize wherein the spectral-transfer time is equal to the dissipation time). In fact, it can make the difference as to whether the dissipation scale is within the range of scalesizes wherein MHD is valid or not.

A. Kraichnan $k^{-3/2}$ Turbulence

In MHD, eddies propagate along the magnetic field at the Alfven speed. Two eddies can only interact during the time that they are passing each other[92,96,97]. Hence, if the Alfven-speed crossing time is less than the eddy turnover time, then the eddy-eddy interaction that would have been completed in an eddy turnover time will be weakened. This is the "Alfven effect" of Kraichnan[88]. When the Alfven effect is in full operation, the spectral transfer of energy proceeds with the timescale

$$\tau_{weak} = \tau_{eddy}^2 / \tau_A \qquad (6)$$

(e.g. eq. (9) of Dobrowolny et al.[98] or eq. (9) of Matthaeus and Zhou[84]). In expression (6) the eddy turnover time is $\tau_{eddy} = L_\perp/u$ and the Alfven crossing time is $\tau_A = L_\parallel/v_A$, where $L_\perp$ and $L_\parallel$ are the perpendicular (to $\underline{B}$) and parallel scalesizes of an eddy, where u is the velocity amplitude of the turbulence at the eddy scalesize $L_\perp$, and where v_A is the Alfven speed of the plasma. Using these τ_{eddy} and τ_A expressions, the spectral energy transfer time (expression (6)) becomes

$$\tau_{weak} = L_\perp^2 v_A / u^2 L_\parallel \qquad . \qquad (7)$$

For the Kraichnan $k^{-3/2}$ cascade, the velocity amplitude of the turbulence scales as $u \propto k_\perp^{-1/4}$ (Refs. 88 and 99), so u can be written $u = u_o L_\perp^{1/4} L_{\perp o}^{-1/4}$, where $L_{\perp o}$ and u_o are the scalesize and velocity amplitude of the large eddies (integral-scale eddies) of the turbulence. Using this expression for u in expression (7) yields the spectral energy transfer timescale

$$\tau_{weak} = v_A L_{\perp o}^{1/2} L_\perp^{3/2} / u_o^2 L_\parallel \qquad (8)$$

for the Kraichnan $k^{-3/2}$ cascade.

For turbulence in a Kraichnan $k^{-3/2}$ cascade, the turbulence will be taken to be mildly anisotropic with $L_\parallel \approx a L_\perp$, where a is a wavenumber-independent constant describing the degree of wavevector anisotropy. For isotropy, $a \approx 1$; for mild anisotropy, a is of order unity. In this case, the spectral energy transfer timescale (expression (8) becomes

$$\tau_{weak} = v_A L_o^{1/2} L_\perp^{1/2} / a u_o^2 \qquad (9)$$

(cf. eq. (8) of Zhou and Matthaeus[99] when $a = 1$). It is expected that the anisotropy will be of the form $a > 1$ (with $L_\parallel > L_\perp$): the larger the value of a, the more-rapid the cascade timescale τ_{weak}.

For Kraichnan turbulence, a turbulence Reynolds number (integral-scale Reynolds number) is constructed from $R_{turb} = \tau_{diss}/ \tau_{spectral-o}$ using expression (9) evaluated at $L_\perp = L_o$ for $\tau_{spectral-o}$ and using $\tau_{diss} = L_o^2/ \nu$: this yields the turbulence Reynolds number

$$R_{turb} = a \, u_o^2 \, L_o / v_A \, \nu \qquad (10)$$

for viscous dissipation acting on Kraichnan turbulence. Here a is the wavevector anisotropy of the turbulence. The larger the value of a, the higher the Reynolds number of the turbulence.

B. Kolmogorov $k^{-5/3}$ Turbulence

Kolmogorov $k^{-5/3}$ turbulence comes about when the spectral transfer of energy is proportional to the local eddy turnover time τ_{eddy} (Ref. 8). For a turbulent cascade with an energy-transfer rate proportional to the local eddy-turnover time, the fluctuation velocity u as a function of scalesize $L_\perp = 1/k_\perp$ in the turbulence goes as $u(L_\perp) \propto L_\perp^{1/3}$ (e.g. Frisch[8]; Appendix of Gary and Borovsky[100]]. Writing $u = C \, L_\perp^{1/3}$, C is obtained by evaluating the expression $u = C \, L_\perp^{1/3}$ at the largest eddy scale $L_{\perp o}$, which gives $C = u_o \, L_{\perp o}^{-1/3}$, with u_o being the largest-eddy fluctuation velocity. Hence $u = u_o \, (L_\perp / L_{\perp o})^{1/3}$. With this expression for u, the eddy turnover time $\tau_{eddy} = L_\perp / u$ becomes

$$\tau_{eddy} = u_o^{-1} L_\perp^{2/3} L_{\perp o}^{1/3} \qquad , \qquad (11)$$

which is plotted as the black curve in Figure 3.

To avoid the Alfven effect for Kolmogorov turbulence, the MHD fluctuations must be on or below the critical-balance curve in $k_\parallel$-$k_\perp$ space shown in Figure 2. The critical-balance curve[93-95] (which is also the boundary of reduced MHD (cf. eq. (0) of Strauss[90]; eq. (6) of Rosenbluth et al.[91]; eq. (6) of Kinney and McWilliams[92]; eq. (8.1) of Biskamp[68]) is defined as the curve in $k_\parallel$-$k_\perp$ space where $\tau_A = \tau_{eddy}$. Equating $\tau_A = L_\parallel / v_A$ with τ_{eddy} given by expression (11) yields the critical-balance-curve expression

$$L_\parallel = L_\perp^{2/3} (\, v_A \, u_o^{-1} \, L_{\perp o}^{1/3}) \qquad , \qquad (12)$$

where the quantity in the parentheses does not vary with scalesize. With $k_\parallel = 1/L_\parallel$ and $k_\perp = 1/L_\perp$ expression (12) can be written in wavevector space.

III. COULOMB SCATTERING

Ion-ion Coulomb collisions can act to spread momentum in a magnetized plasma, producing a shear viscosity. For a "collisionless" plasma the Coulomb-collision mean free path is longer than any fluid scalesize of interest to MHD turbulence, so a Coulomb-scattering viscosity acting on flows in the parallel-to-$\underline{B}$ direction is meaningless since momentum transport is not proportional to a gradient. For examples, using eq. (6.4.11) of Krall and Trivelpiece[101] for the ion-ion collision time yields

$$\tau_{ii} = 0.28 \, m_i^{1/2} \, (k_B T_i)^{3/2} / n \, e^4 \, \log_e(\Lambda) \qquad (13)$$

where eq. (6.2.7) of Krall and Trivelpiece[92] gives

$$\Lambda = 3 \, (k_B T_e)^{3/2} / 2\pi n^{1/2} e^3 \qquad . \qquad (14)$$

Using the parameters of Table I in expressions (13) and (14), the ion-ion momentum-exchange collision time τ_{ii} is $\tau_{ii} = 1.6\times10^6$ sec = 19 days for the solar wind at 1 AU, $\tau_{ii} = 1.6\times10^8$ sec = 5 years for the Earth's magnetosheath, and $\tau_{ii} = 4.8\times10^{11}$ sec = 15,000 years for the Earth's plasma sheet. Multiplying these times by the ion thermal velocity to get collisional mean free paths yields 4.2×10^{12} cm = 0.28 AU for the solar wind at 1 AU, 3.1×10^{15} cm = 206 AU for the Earth's magnetosheath, and 3.3×10^{19} cm = 11 parsec for the Earth's plasma sheet. For the solar wind the mean free path of 4.2×10^{12} cm is 280 times longer than the 1.5×10^{10} cm large-eddy scale of the turbulence; for the magnetosheath and the plasma sheet these mean free paths are vastly larger than the plasmas themselves.

Perpendicular to the magnetic field, the gyrational motion of the particles about the field lines holds the plasma particles together allowing a fluid-like behavior. Coulomb scattering acts to disrupt this gyrational motion, displacing guiding centers and spreading momentum. This produces a shear viscosity[24,102] and also a cross-field conductivity[15,25,26]. Analyzing the effects of particle-particle collisions on the stress tensor of a magnetized plasma, Braginskii[22] obtains 5 transport coefficients η_0, η_1, η_2, η_3, and η_4 relating the terms of the stress tensor to the terns of the rate-of-strain tensor. The coefficient that pertains to shear viscosity strictly perpendicular to $\underline{B}$ (Type-II motion of Kaufman[24]) is η_1 (expression (2.23) of Braginskii[22]). The coefficient η_2 is a shear viscosity pertaining to flow in the parallel-to-$\underline{B}$ direction or pertaining to flow gradients in the parallel-to-$\underline{B}$ direction. The coefficient η_0 (which is $\omega_{ci}^2\tau_{ii}^2$ times larger than η_1) acts on compressive elements of the rate-of-strain tensor in a magnetized plasma, as a bulk viscosity

would. The coefficients η_3 and η_4 (which are $\omega_{ci}\tau_{ii}$ times larger than η_1) are Hall terms acting perpendicular to the flow velocities that do not dissipate energy.

Braginskii's expression for the Coulomb-scattering perpendicular shear viscosity is (eq. (2.23) of Braginskii[22] and see also eq. (16) of Simon[103])

$$\nu_{Brag} = (3/10)\, r_{gi}^2 / \tau_{ii}. \qquad , \qquad (15)$$

which has the functional form of a lengthscale squared divided by a timescale. Here r_{gi} is a thermal-ion gyroradius and τ_{ii} is the ion-ion collision time. Evaluating expression (15) for the parameters of the magnetized plasmas in Table I and using the values of τ_{ii} calculated above from expression (13) yields $\nu_{Brag} = 3.8\times10^6$ cm^2/sec for the solar wind at 1 AU, $\nu_{Brag} = 1.3\times10^5$ cm^2/sec for the Earth's magnetosheath, and $\nu_{Brag} = 3.3\times10^3$ cm^2/sec for the Earth's plasma sheet. These values are entered into Table I. For comparison, the kinematic viscosity of cold water is 1.8×10^{-2} cm^2/sec and of STP air is 1.7×10^{-4} cm^2/sec.

Owing to the perpendicular shear viscosity, a flow shear perpendicular to $\underline{B}$ will spread with time according to $\partial\underline{\omega}/\partial t = \nu_{Brag}\,\partial^2\underline{\omega}/\partial x^2$ where $\underline{\omega}$ is the vorticity $\nabla\times\underline{v}$ (parallel to $\underline{B}$). This expression yields a viscous-spreading timescale τ_{Brag} given by

$$\tau_{Brag} = L^2/\nu_{Brag} \qquad . \qquad (16)$$

In the top panel of Figure 3, the Braginskii viscous timescale τ_{Brag} given by expression (16) is plotted in green as a function of the scalesize L for typical solar-wind parameters.

The spectral transfer time τ_{eddy} for Kolmogorov turbulence (expression (11)) is plotted as the black curve in Figure 3 and the spectral transfer time τ_{weak} for Kraichnan turbulence (expression (9)) is plotted as the gray curve. As can be seen by comparing the green, black, and gray curves in the top panel of Figure 3, for all of the values of L plotted the Braginskii viscous timescale τ_{Brag} is greater than the Kolmogorov-turbulence spectral-transfer time τ_{eddy} and the Kraichnan-turbulence spectral-transfer time τ_{weak}.

For typical parameters of the Earth's magnetosheath (see Table I) the value of the Braginskii shear viscosity is $\nu_{Brag} = 1.3\times10^5$ cm^2/sec and for typical parameters of the Earth's magnetotail plasma sheet (see Table I) the value of the Braginskii shear viscosity is $\nu_{Brag} = 3.3\times10^3$ cm^2/sec. Using these values in expression (16), the Braginskii viscous timescale τ_{Brag} is plotted as the green curves in the second and third panels of Figure 3. Also plotted in those two panels as the black curves is the eddy-turnover time τ_{eddy} as a function of the eddy size L and as

the gray curves the Kraichnan-turbulence spectral-transfer time τ_{weak} as a function of the eddy size L. As can be seen by comparing the green, black, and gray curves in the second and third panels, for all of the values of L plotted the Braginskii viscous timescale τ_{Brag} is greater than the eddy-turnover time and the spectral-transfer time.

For Kolmogorov turbulence, a turbulence Reynolds number is constructed from expression (5) with expression (16) for τ_{Brag} and with $\tau_{spectral-o} = \tau_{eddy-o} = L_o/u_o$ yields

$$R_{turb-Brag} = L_o u_o / \nu_{Brag} , \tag{17}$$

where L_o is the large-eddy scalesize, u_o is the fluctuation amplitude of the turbulence, and ν_{Brag} is given by expression (15). Using the three values of ν_{Brag} calculated above for the three plasmas and using the parameters of Table I yields turbulence Reynolds numbers of $R_{turb-Brag} = 1.0 \times 10^9$ for Kolmogorov turbulence in the solar wind, $R_{turb-Brag} = 2.5 \times 10^{10}$ for Kolmogorov turbulence in the magnetosheath, and $R_{turb-Brag} = 2.3 \times 10^{12}$ for Kolmogorov turbulence in the plasma sheet. These values are entered into Table I.

For Kraichnan turbulence, a turbulence Reynolds number is constructed from expression (5) with expression (16) for τ_{Brag} and with $\tau_{spectral} = \tau_{weak} = v_A L_o / u_o^2$ (from expression (9) evaluated at $L = L_o$) yields

$$R_{turb-Brag} = a\, L_o u_o^2 / v_A \nu_{Brag} , \tag{18}$$

where L_o is the large-eddy scalesize, u_o is the fluctuation amplitude of the turbulence, v_A is the Alfven speed of the plasma, a is the wavevector-anisotropy parameter $L_\parallel \approx a\, L_\perp$, and ν_{Brag} is given by expression (15). The larger the value of the anisotropy factor a, the higher the Reynolds number of the turbulence. Using the three values of ν_{Brag} calculated above for the three plasmas, taking $a = 1$, and using the parameters of Table I yields turbulence Reynolds numbers of $R_{turb-Brag} = a \cdot 1.8 \times 10^8$ for Kraichnan turbulence in the solar wind, $R_{turb-Brag} = a \cdot 9.0 \times 10^9$ for Kraichnan turbulence in the magnetosheath, and $R_{turb-Brag} = a \cdot 4.3 \times 10^{11}$ for Kraichnan turbulence in the plasma sheet. These values are entered into Table I.

IV. ELECTRON AND ION LANDAU DAMPING

Shear viscosity acts to spatially spread a shear structure in a fluid by first damping out the higher-wavenumber Fourier modes describing the shear and later damping out the lower-wavenumber Fourier modes. In this section it is noted that Landau damping acts in this precise fashion for a shear flow perpendicular to a magnetic field in a collisionless plasma, with that shear flow spreading along the magnetic-field direction as a shear Alfven wave. By analyzing the Landau damping, a shear-viscosity coefficient for collisionless plasma will be obtained.

For turbulence in a magnetized plasma, every flow perturbation normal to $\underline{B}$ has two aspects: an eddy aspect and an Alfven-wave aspect (Sect. 3.6 of Alfven and Falthammar[15]; Refs. 87 and 88). Eddies are not stationary in a magnetized plasma: an eddy propagates along the magnetic field at the Alfven velocity. The Alfven-wave aspect complicates eddy-eddy interactions in turbulence[84,88]. The Alfven-wave aspect also introduces dissipation of the turbulent fluctuations in a collisionless plasma via wave-particle interactions.

In a collisionless magnetized plasma, all Alfven waves are subject to dissipation via Landau damping[104-106]. Longer-wavelength waves have longer lifetimes, so the dissipation timescales for larger-scalesize turbulent fluctuations are longer than the dissipation timescales for the smaller-scalesize fluctuations.

Landau damping of Alfven waves in a collisionless plasma operates as follows. Every Alfven wave with a nonzero $k_\perp$ has a parallel electric field $E_\parallel$ (e.g. Refs. 18 and 107). Particles of the plasma moving near the Alfven speed effectively interact with the $E_\parallel$ of the wave via the Landau resonance; the waves give energy to the particles and dissipate. This wave dissipation results in a parallel heating of the Landau-resonant species. The larger the values of $k_\perp$ and $k_\parallel$, the stronger the wave's $E_\parallel$, and the stronger the wave-particle interactions, hence the stronger the damping.

In Figure 4 the electron and ion distribution functions f(v) for a Maxwellian plasma with $T_i = T_e$ are plotted (solid curves) as a function of $v_\parallel/v_{Ti}$. Also plotted (dashed curves) is vf(v), which is the $\partial f/\partial v$ factor in the Landau-damping decrement (cf. Sect. 6.5 of Nicholson[108]). Waves that have phase velocities less than $v_{Ti}/2^{1/2}$ (Region 1 in the figure) are in Landau resonance with both electrons and ions. Waves that have phase velocities greater than $v_{Ti}/2^{1/2}$ but less than $v_{Te}/2^{1/2}$ (Region 2 in the figure) are in Landau resonance with electrons but not ions. Waves that have phase velocities $> v_{Te}/2^{1/2}$ (Region 3 in the figure) are not in Landau resonance

with either the electrons or the ions. For Alfven waves, the plasma β and temperature ratio T_e/T_i determine the Alfven speed relative to the ion and electron thermal speeds. The range of β values pertaining to Regions 1, 2, and 3 are noted in Figure 4.

It is argued here that linear-Vlasov theory (see Ref. 109) can be used to quantify the damping of MHD-turbulence fluctuations of all scalesizes in a collisionless plasma. At long wavelengths (large scalesizes) where the fluctuation amplitudes can be large, the Landau damping will be very weak and the perturbations of the particle orbits by the Alfven waves will be very weak. This is indeed the case for comparisons of numerically simulated Alfven waves with linear Vlasov theory (e.g. Fig. 4 of Ref. 110 or Fig. 11 of Ref. 111, and see also Refs. 112 and 113). This is unlike the cases of large-amplitude Langmuir waves and large-amplitude ion-acoustic waves where particle trapping by the waves would invalidate linear-Vlasov calculations (cf. Sects. 6.7 and 6.8 of Ref. 108). At short wavelengths (small scalesizes) where Landau damping can be strong the amplitudes of the MHD fluctuations are small and the linear theory should be valid.

As a consequence of Landau damping, the amplitude of an Alfven wave decreases with time t as $e^{-\gamma t}$, where γ is the "damping decrement". The damping time (e-folding time for the amplitude) is $\tau_{damp} = -1/\gamma$. The Landau damping decrement for Alfven waves has been analytically calculated with approximations[104-106,114] and was numerically calculated from the linear Vlasov equation without approximation by Gary and Borovsky[100,115]. The Landau-damping decrement for Alfven waves can be written in the form

$$\gamma = -A\,\omega_{pe}\,(k_\parallel\,\lambda_{De})\,(k_\perp c/\omega_{pe})^2 \qquad , \qquad\qquad (19)$$

(cf. eqs. (13b) and (19b) of Stefant[97] and eq. (5) of Gary and Borovsky[91]), where $\omega_{real} = k_\parallel v_A$ has been used. In expression (19) $k_\perp$ is the component of the wavevector $\underline{k}$ that is perpendicular to the ambient magnetic field in the plasma, $k_\parallel$ is the component of the wavevector $\underline{k}$ that is parallel to the magnetic field in the plasma, ω_{pe} is the electron plasma frequency, λ_{De} is the electron Debye length, and c/ω_{pe} is the electron skin depth. In expression (19), A is a parameter that depends on the beta value β of the plasma and on the electron-to-ion temperature ratio T_e/T_i. Using numerical solutions to the Vlasov-Maxwell equations (cf. Gary[109]), the parameter A is plotted as a function of β in Figure 5 for a plasma with $T_e = T_i$, a hot-electron plasma with $T_e = 10T_i$, and a hot-ion plasma with $T_i = 10T_e$. As can be seen in Figure 5, at very low β (Region 3) the values of $A \to 0$ reflecting no Landau damping of the Alfven waves owing to $v_A \gg v_{Te}$ in

Region 3. In Region 2 where $v_{Te} > v_A > v_{Ti}$ the value of A is A ≈ 1 reflecting electron Landau damping of the Alfven waves. For β values near the transition from Region 2 to Region 3 the value of A has a local maximum where the Alfven speed v_A in the plasma and the ion-acoustic speed C_s in the plasma are approximately equal. This $v_A = C_s$ equality occurs when $\beta_i + 3\beta_e = 2$, where $\beta_e = 8\pi nk_BT_e/B^2$ and $\beta_i = 8\pi nk_BT_i/B^2$. This resonance at $v_A = C_s$ was pointed out by Stefant[91]. We speculate that the enhanced (electron) Landau damping in this resonance is caused by a merging of the ion-acoustic and Alfven branches of the plasma dispersion relation, producing an Alfven wave with an extra-strong parallel electric field producing enhanced wave-particle interactions with the electrons of the plasma. In Region 1 where Alfven waves are in Landau resonance with ions the value of A increases with plasma β as $A \propto \beta^1$. Ion Landau damping (interaction of ions with $\delta E_\parallel$ of the wave) predicts $A \approx (m_i/m_e)^{1/2}$ in Region 1 (Ref. 106), as indicated by the purple curve in Figure 5. However, the Stefant[97] theoretical analysis assumed $\delta B_\parallel = 0$ for the Alfven waves, precluding transit-time damping. The analysis of Gary and Borovsky[100,115] demonstrated that ion transit-time damping (interaction of ions with $\delta B_\parallel$ at the Landau resonance) dominates the classical ion Landau damping (interaction of ions with $\delta E_\parallel$ at the Landau resonance) for Alfven waves in a high-β plasma. Note in Figure 5, in the lower-β regions the value of A matches the coefficients of eqs. (13b) and (19b) of Stefant[106] and eq. (5) of Gary and Borovsky[100].

For an A value for the solar-wind plasma with β ≈ 1.5, the $T_e = T_i$ curve of Figure 5 yields A ~ 3. For the magnetosheath plasma with β ≈ 7.5 the $T_i = 10T_e$ curve of Figure 5 yields A ~ 80. And for the plasma-sheet plasma with β ≈ 7 the $T_i = 10T_e$ curve of Figure 5 yields A ~ 70. These A values are inserted into Table I.

Using $k_\parallel = 1/L_\parallel$ and $k_\perp = 1/L_\perp$, where $L_\parallel$ and $L_\perp$ are the parallel and perpendicular gradient scalesizes of an eddy with wavenumber $(k_\parallel, k_\perp)$, and using $\lambda_{De}\omega_{pe} = v_{Te}$, expression (19) gives for $\tau_{Landau} = -1/\gamma$

$$\tau_{Landau} = A^{-1} v_{Te}^{-1} \omega_{pe}^2 c^{-2} L_\parallel L_\perp^2 \qquad . \tag{20}$$

To use expression (20) to construct a turbulence Reynolds number, an estimate of the parallel-to-<u>B</u> scalesize $L_\parallel$ of a large eddy must be made. Depending on whether Kolmogorov or Kraichnan turbulence is being considered, the estimate of $L_\parallel$ as a function of $L_\perp$ will differ.

For Kolmogorov turbulence (see Section II.B) the assumption will be made that the turbulence is in the middle of the reduced-MHD regime where $\tau_A = L_{\parallel}/v_A = 2\tau_{eddy}$, which gives a parallel-to-$\underline{B}$ gradient scale $L_{\parallel} = 2\tau_{eddy} \, v_A$, where τ_{eddy} is the eddy turnover time (eddy rotation period) and v_A is the Alfven speed of the plasma. Using $L_{\parallel} = 2\tau_{eddy} \, v_A$ in expression (20) yields

$$\tau_{Landau} \; = \; 2 \, A^{-1} \, v_{Te}^{-1} \, \omega_{pe}^2 \, c^{-2} \, \tau_{eddy} \, v_A \, L_{\perp}^2 \qquad . \tag{21}$$

Note that expression (21) pertains to MHD fluctuations in the reduced-MHD regime below the critical-balance curve and that τ_{eddy} in expression (21) is the eddy turnover time for an eddy of size $L_{\perp}$. Using expression (11) for τ_{eddy}, expression (21) yields

$$\tau_{Landau} \; = \; 2 \, A^{-1} \, v_{Te}^{-1} \, \omega_{pe}^2 \, c^{-2} \, v_A \, L_{\perp}^{8/3} \, L_{\perp o}^{1/3} \, u_o^{-1} \tag{22}$$

for the dissipation time owing to Landau damping.

For Kraichnan turbulence (see Section II.A) the assumption will be made that the turbulence is mildly anisotropic with $L_{\parallel} = aL_{\perp}$, where a is an order-unity constant independent of scalesize $L_{\perp}$. With this the Landau-damping dissipation timescale given by expression (20) becomes

$$\tau_{Landau} \; = \; a \, \omega_{pe}^2 \, L_{\perp}^3 \, / \, A \, v_{Te} \, c^2 \qquad . \tag{23}$$

Note that expression (23) pertains to MHD fluctuations in a spectrum that is mildly anisotropic. The higher the value of the wavevector-anisotropy factor a, the longer the timescale for Landau damping.

For typical solar-wind parameters ($T_i = 7$ eV and $B = 6$ nT) and for $A \sim 3$ (see Figure 5), the value of the Landau-damping dissipation time given by expression (22) for Kolmogorov turbulence is $\tau_{Landau} = 3.6 \times 10^{-15} \, L_{\perp}^{8/3}$ where $L_{\perp}$ is in cm and τ_{Landau} is in seconds. In the top panel of Figure 3, the Landau-damping dissipation time is τ_{Landau} is plotted in blue as a function of the scalesize $L_{\perp}$ for typical solar-wind parameters. And for typical solar-wind parameters, the value of the Landau-damping dissipation time given by expression (23) for Kraichnan turbulence is $\tau_{Landau} = a \cdot 4.4 \times 10^{-20} \, L^3$ where L is in cm and τ_{Landau} is in sec. In the top panel of Figure 3, the Landau-damping dissipation time is τ_{Landau} for Kraichnan turbulence with $a = 1$ is plotted in light-blue as a function of the scalesize $L_{\perp}$ for typical solar-wind parameters. Plotted in black in the top panel of Figure 3 is the spectral-transfer time τ_{eddy} (expression (11)) for a Kolmogorov-turbulence eddy of size $L_{\perp}$ in the solar wind and plotted in gray in the top panel of Figure 3 is the spectral-transfer time τ_{weak} (expression (9)) for a Kolmogorov-turbulence eddy of size $L_{\perp}$ in the

solar wind. As can be seen by comparing the blue and black curves, for $L_\perp > 15$ km the Landau-damping time τ_{Landau} is greater than the eddy-turnover time. At $L_\perp = 15$ km the two times are equal: $\tau_{Landau} = \tau_{eddy}$. Here, for dissipation by Landau damping, the Kolmogorov $k^{-5/3}$ turbulence in the solar wind would have a Kolmogorov dissipation scale $L_{Kol-Landau} = 15$ km. Note that this Kolmogorov scale for Landau damping is smaller then the minimum scale for MHD in the solar wind (i.e. it is smaller than ion skin depths and ion gyroradii), so the Kolmogorov MHD-turbulence cascade will not reach the Landau-damping Kolmogorov scale in the solar wind. As can be seen by comparing the light-blue and gray curves in the top panel of Figure 3, for $L_\perp >$ 800 km the Landau-damping time τ_{Landau} is greater than τ_{weak}. At $L_\perp = 800$ km the two times are equal: $\tau_{Landau} = \tau_{weak}$. Here, for dissipation by Landau damping, the Kraichnan $k^{-3/2}$ turbulence in the solar wind would have a Kolmogorov dissipation scale $L_{Kol-Landau} = 800$ km. Note that this Kolmogorov scale for Landau damping is larger then the minimum scale for MHD in the solar wind, so the Kraichnan MHD-turbulence cascade will reach the Landau-damping Kolmogorov scale in the solar wind.

For typical parameters of the Earth's magnetosheath and plasma sheet (see Table I) and for A=80 (magnetosheath) and A=70 (plasma sheet) the Kolmogorov-turbulence Landau-damping dissipation time given by expression (22) is $\tau_{Landau} = 1.6 \times 10^{-19} L_\perp^{8/3}$ for the magnetosheath and $\tau_{Landau} = 1.5 \times 10^{-21} L_\perp^{8/3}$ for the plasma sheet, where $L_\perp$ is in cm and τ_{Landau} is in sec. The Kolmogorov-turbulence Landau-damping dissipation timescale τ_{Landau} is plotted as the blue curves in the second and third panels of Figure 3. Also plotted in those two panels as the black curves is the eddy-turnover time τ_{eddy} as a function of the eddy size $L_\perp$ from expression (11). As can be seen in the second panel, $\tau_{Landau} = \tau_{eddy}$ at $L = 38$ km in the magnetosheath, which means the Kolmogorov dissipation scale for Kolmogorov $k^{-5/3}$ turbulence in the magnetosheath is $L_{Kol-Landau} = 38$ km for dissipation by Landau damping diffusion. And as can be seen in the third panel of Figure 4, $\tau_{Landau} = \tau_{eddy}$ at $L = 300$ km in the plasma sheet, which means the Kolmogorov dissipation scale for Kolmogorov turbulence in the plasma sheet is $L_{Kol-Landau} = 300$ km for dissipation by Bohm diffusion. Note that for both of these plasmas, the Kolmogorov scales for Landau damping is smaller then the minimum scale for MHD in the plasmas (i.e. than ion skin depths and ion gyroradii), so the Kolmogorov-turbulence MHD-turbulence cascade will not reach the Landau-damping Kolmogorov scales in these two plasmas.

For typical parameters of the Earth's magnetosheath and plasma sheet (see Table I) the Kraichnan-turbulence Landau-damping dissipation time given by expression (23) is $\tau_{Landau} = a \cdot 3.2 \times 10^{-21} L^3$ for the magnetosheath and $\tau_{Landau} = a \cdot 1.4 \times 10^{-23} L^3$ for the plasma sheet, where L is in cm and τ_{Landau} is in sec. The Kraichnan-turbulence Landau-damping dissipation timescale τ_{Landau} is plotted for $a = 1$ as the light-blue curves in the second and third panels of Figure 3. Also plotted in those two panels as the gray curves is the spectral-transfer time τ_{weak} for Kraichnan $k^{-3/2}$ turbulence as a function of the eddy size $L_\perp$ from expression (9). As can be seen in the second panel, $\tau_{Landau} = \tau_{weak}$ at L = 330 km in the magnetosheath, which means the Kolmogorov dissipation scale for Kraichnan $k^{-3/2}$ turbulence in the magnetosheath is $L_{Kol-Landau} =$ 330 km for dissipation by Landau damping diffusion. And as can be seen in the third panel of Figure 4, $\tau_{Landau} = \tau_{weak}$ at L = 1350 km in the plasma sheet, which means the Kolmogorov dissipation scale for Kraichnan turbulence in the plasma sheet is $L_{Kol-Landau} =$ 1350 km for dissipation by Bohm diffusion. Note that for both of these plasmas, the Kolmogorov scales for Landau damping is larger then the minimum scale for MHD in the plasmas (i.e. than ion skin depths and ion gyroradii), so the Kraichnan-turbulence MHD-turbulence cascade will not reach the Landau-damping Kolmogorov scales in these two plasmas.

Note that the functional form of Landau damping is in the form of a hyperviscosity, that is, a viscosity that has a wavenumber dependence k^α with $\alpha > 0$ (cf. Refs. 116 and 117). For ordinary viscosity ν which is a constant, with $\partial\omega/\partial t = \nu\partial^2\omega/\partial x^2$ (where ω is the vorticity) the dissipation time $\tau = \nu^{-1}L^2$ varies as $\tau \propto L^2$. Comparing the expression $\tau = \nu^{-1}L^2$ with expression (20), the kinematic shear viscosity associated with Landau damping is

$$\nu_{Landau} = A\, v_{Te}\, c^2\, \omega_{pe}^{-2}\, L_\parallel^{-1} \quad , \tag{24}$$

which is not a constant (it varies with $L_\parallel$). Viscosity can be expressed as a lengthscale squared divided by a timescale. In the electron-Landau-damping regime ($10^{-4} < \beta_e < 1$) where $A \approx 1$ (see Figure 5), expression (24) can be written

$$\nu_{Landau} = (c/\omega_{pe})^2 / \tau_{transit-e} \tag{25}$$

where $\tau_{transit-e} \equiv L_\parallel/v_{Te}$ is the time required for a thermal electron to transit one parallel wavelength of the Alfven wave. In the ion-transit-time-damping regime ($\beta_i > 1$) where $A \sim 10\, \beta_i$ (see Figure 5), expression (24) can be written

$$\nu_{Landau} \approx (T_e/4T_i)^{1/2}\, r_{gi}^2 / \tau_{transit-i} \tag{26}$$

where $\tau_{transit-i} \equiv L_{\parallel}/v_{Ti}$ is the time required for a thermal ion to transit one parallel wavelength of the Alfven wave.

If the Alfvenic fluctuations of the MHD turbulence are in the reduced-MHD regime on or below the critical-balance curve (Kolmogorov $k^{-5/3}$ turbulence) then expression (22) holds; comparing expression (22) with $\tau = \nu^{-1} L^2$ yields

$$\nu_{Landau} = 2^{-1} A L_{\perp o}^{-1/3} v_{Te} c^2 \omega_{pe}^{-2} u_o v_A^{-1} L_{\perp}^{-2/3} \qquad , \qquad (27)$$

for the kinematic shear viscosity of MHD fluctuations associated with Landau damping. For the Kolmogorov MHD turbulence, Landau damping acts like a shear viscosity $\nu \propto L_{\perp}^{-2/3}$ (or equivalently $\nu \propto k_{\perp}^{2/3}$) that is stronger at smaller scales (see also Cranmer and Ballegooijen[118]). If the Alfvenic fluctuations of the MHD turbulence are mildly anisotropic (Kraichnan $k^{-3/2}$ turbulence) then expression (23) holds; comparing expression (23) with $\tau = \nu^{-1} L^2$ yields

$$\nu_{Landau} = A v_{Te} c^2 \omega_{pe}^{-2} L_{\perp}^{-1} a^{-1} , \qquad (28)$$

for the kinematic shear viscosity of mildly anisotropic MHD fluctuations associated with Landau damping. For the Kraichnan MHD turbulence, expression (28) indicates that Landau damping acts like a shear viscosity $\nu \propto L^{-1}$ (or equivalently $\nu \propto k$) that is stronger at smaller scales. Expression (28) indicates that the larger the wavevector-anisotropy factor a, the weaker the Landau-damping shear viscosity.

For Kolmogorov $k^{-5/3}$ turbulence, expression (21) used in the numerator of expression (4) yields the expression for the turbulence Reynolds number of a large eddy of scalesize $L_{\perp o}$

$$R_{turb-Landau} = 2 A^{-1} v_{Te}^{-1} \omega_{pe}^2 c^{-2} v_A L_{\perp o}^2 \qquad (29)$$

where Landau damping in the collisionless plasma is acting on the fluctuations of the turbulence. Expression (29) has a reduced-MHD assumption in it: the larger the value of the anisotropy factor a, the higher the Reynolds number of the turbulence. In expression (29) the value of A depends on the plasma β (see Figure 5). Using Figure 5, A~3 for the solar wind, A~80 for the magnetosheath, and A~70 for the plasma sheet. Evaluating expression (29) for the parameters of Table I with these A values yields $R_{turb-Landau} = 1.1\times10^8$ for Kolmogorov turbulence in the solar wind, $R_{turb-Landau} = 4.4\times10^4$ for Kolmogorov turbulence in the magnetosheath, and $R_{turb-Landau} = 1100$ for Kolmogorov turbulence in the plasma sheet. These values are entered into Table I. Recall that these Reynolds numbers are the ratios of the Landau-damping dissipation time for large eddies to the dynamical time for large eddies.

For Kraichnan $k^{-3/2}$ turbulence, expression (23) for $\tau_{diss} = \nu_{Landau}^{-1}$ used in the numerator of expression (5) with expression (9) in the denominator, evaluated at $L_\perp = L_{\perp o}$, yields the expression for the turbulence Reynolds number of a large eddy of scalesize $L_{\perp o}$

$$R_{turb\text{-}Landau} = (a^2/A)\,(L_{\perp o}^2\omega_{pe}^2/c^2)\,(u_o^2/v_{Te}v_A) \tag{30}$$

where Landau damping in the collisionless plasma is acting on the fluctuations of the turbulence. Note that the right hand side of expression (30) is $u_o^2/2a^2v_A^2$ times the right hand side of expression (29), i.e. the turbulence Reynolds number for Kraichnan turbulence is $u_o^2/2a^2v_A^2$ times the turbulence Reynolds number for Kolmogorov turbulence. Expression (30) has a mildly anisotropic-turbulence assumption in it. In expression (30) the value of A depends on the plasma β (see Figure 5). Using Figure 5, A~3 for the solar wind, A~80 for the magnetosheath, and A~70 for the plasma sheet. Evaluating expression (30) for the parameters of Table I with these A values yields $R_{turb\text{-}Landau} = a^2 \cdot 4.6 \times 10^5$ for Kraichnan turbulence in the solar wind, $R_{turb\text{-}Landau} = a^2 \cdot 2940$ for Kraichnan turbulence in the magnetosheath, and $R_{turb\text{-}Landau} = a^2 \cdot 19.4$ for Kraichnan turbulence in the plasma sheet. These values are entered into Table I. Recall that these Reynolds numbers are the ratios of the Landau-damping dissipation time for large eddies to the spectral-transfer time for large eddies.

As will be seen in Section VI, for Landau-damping dissipation the standard Reynolds-number scaling of characteristic scalesizes will not hold.

V. BOHM DIFFUSION

In laboratory experiments, cross-field gradients are often observed to spread at the Bohm-diffusion rate (Refs. 119 and 120; Fig. 5-20 of Ref. 121). Bohm diffusion could be thought of as the fastest possible diffusion in a magnetized plasma, acting with a stepsize equal to a particle gyroradius and a timestep equal to a particle gyroperiod. In various situations the mechanism underlying Bohm diffusion has been attributed to thermal electromagnetic fluctuations[122], field-line wandering[123], stochastic $\underline{E} \times \underline{B}$ drifts[124,125], turbulent electric fields[126,127], and drift waves[128,129].

The Bohm diffusion coefficient D_B is given by the standard expression

$$D_B = c\, k_B\, T_i / 16\, e\, B \qquad\qquad (31)$$

(e.g. eq. (74) of Bohm et al.[119] or eq. (1.14.5) of Krall and Trivelpiece[101]) where the factor 1/16 in expression (31) is arguable. Values of D_B are entered into Table I. Taking the kinematic shear viscosity (momentum diffusion) to be approximately D_B (mass diffusion) and expressing D_B in the form of a lengthscale squared divided by a timescale yields

$$\nu_{Bohm} = (1/16)\, r_{gi}^2 / \tau_{ci} \qquad\qquad (32)$$

where r_{gi} is a thermal-ion gyroradius and τ_{ci} is the ion cyclotron period $2\pi/\omega_{ci}$. Inserting this Bohm-diffusion coefficient into a diffusion equation $\partial f/\partial t = D_B \partial^2 f/\partial x^2$ yields a Bohm-diffusion timescale

$$\tau_{Bohm} = L^2/D_B \qquad\qquad , \qquad\qquad (33)$$

where L is a gradient lengthscale. This is the timescale for a gradient of scalesize L to spread; this spreading occurs by the dissipation of high-k modes in the Fourier description of the gradient, so τ_{Bohm} is a dissipation timescale for gradients of scalesize L.

For typical solar-wind parameters ($T_i = 7$ eV and $B = 6$ nT), the value of the Bohm diffusion coefficient is $D_B = 7.3 \times 10^{11}$ cm^2/sec. In the top panel of Figure 3, the Bohm diffusion timescale τ_{Bohm} given by expression (33) is plotted in red as a function of the scalesize L for typical solar-wind parameters. Plotted in black in the top panel of Figure 3 is the spectral-transfer time τ_{eddy} for a Kolmogorov-turbulence eddy of size L in the solar wind as given by expression (11) and plotted in gray in the top panel of Figure 3 is the spectral-transfer time τ_{weak} for a Kraichnan-turbulence eddy of size L in the solar wind as given by expression (9). As can be seen by comparing the red and black curves, for $L > 100$ km the Bohm diffusion time τ_{Bohm} is greater than the eddy-turnover time. At $L = 100$ km the two times are equal: $\tau_{Bohm} = \tau_{eddy}$. Here, for

dissipation by Bohm diffusion, Kolmogorov turbulence in the solar wind turbulence would have a Kolmogorov dissipation scale $L_{Kol-Bohm}$ = 100 km. And as can be seen by comparing the red and gray curves, for L > 1600 km the Bohm diffusion time τ_{Bohm} is greater than the spectral-transfer time τ_{weak}. At L = 1600 km the two times are equal: $\tau_{Bohm} = \tau_{weak}$. Here, for dissipation by Bohm diffusion, isotropic (a = 1) Kraichnan turbulence in the solar wind turbulence would have a Kolmogorov dissipation scale $L_{Kol-Bohm}$ = 1600 km.

For typical parameters of the Earth's magnetosheath (see Table I) the value of the Bohm diffusion coefficient is D_B = 1.0×10^{13} cm^2/sec and for typical parameters of the Earth's magnetotail plasma sheet (see Table I) the value of the Bohm diffusion coefficient is D_B = 3.1×10^{14} cm^2/sec. Using these values in expression (33), the Bohm-diffusion timescale τ_{Bohm} is plotted as the red curves in the second and third panels of Figure 3. Also plotted in those two panels as the black curves is the spectral-transfer time τ_{eddy} as a function of the eddy size L and as the gray curves is the spectral-transfer time τ_{weak} as a function of the eddy size L. As can be seen in the second panel, $\tau_{Bohm} = \tau_{eddy}$ at L = 100 km in the magnetosheath, which means the Kolmogorov dissipation scale for Kolmogorov turbulence in the magnetosheath is $L_{Kol-Bohm}$ = 100 km for dissipation by Bohm diffusion. And as can be seen in the third panel of Figure 4, $\tau_{Bohm} = \tau_{eddy}$ at L = 1000 km in the plasma sheet, which means the Kolmogorov dissipation scale for Kolmogorov turbulence in the plasma sheet is $L_{Kol-Bohm}$ = 1000 km for dissipation by Bohm diffusion. And as can be seen in the second panel, $\tau_{Bohm} = \tau_{weak}$ at L = 340 km in the magnetosheath, which means the Kolmogorov dissipation scale for Kraichnan turbulence in the magnetosheath is $L_{Kol-Bohm}$ = 340 km for dissipation by Bohm diffusion. And as can be seen in the third panel of Figure 4, $\tau_{Bohm} = \tau_{weak}$ at L = 3700 km in the plasma sheet, which means the Kolmogorov dissipation scale for isotropic (a = 1) Kraichnan turbulence in the plasma sheet is $L_{Kol-Bohm}$ = 3700 km for dissipation by Bohm diffusion.

The Bohm-diffusion timescale applied to a large eddy can be used in the numerator of expression (4) to construct a turbulence Reynolds number $R_{turb} = \tau_{Bohm}/\tau_{eddy}$. Using expression (33) for τ_{Bohm} and $\tau_{eddy} = L_o/u_o$ thus yields

$$R_{turb-Bohm} = L_o u_o / D_B \tag{34}$$

for strongly anisotropic Kolmogorov k$^{-5/3}$ turbulence. Using expression (31) for D_B, the turbulence Reynolds number (34) can be written as

$$R_{\text{turb-Bohm}} \;=\; 16 \,(u_o/v_{Ti})\,(L_o/r_{gi}) \qquad\qquad . \tag{35}$$

Evaluating expression (35) for Kolmogorov $k^{-5/3}$ turbulence in the solar wind at 1 AU gives $R_{\text{turb-Bohm}} = 1.0 \times 10^4$, for the Earth's magnetosheath it gives $R_{\text{turb-Bohm}} = 325$, and for the Earth's plasma sheet it gives $R_{\text{turb-Bohm}} = 25$. These values are entered into Table I.

For mildly anisotropic Kraichnan turbulence, using expression (33) for $\tau_{\text{diss}} = \tau_{\text{Bohm}}$ and expression (9) for $\tau_{\text{spectral-o}} = \tau_{\text{weak}}$ evaluated at $L_\perp = L_{\perp o}$ in expression (5) for the Kraichnan-turbulence turbulence Reynolds number yields

$$R_{\text{turb-Bohm}} \;=\; a\, L_{\perp o}\, u_o^{\,2} \,/\, v_A\, D_B \tag{36}$$

for Kraichnan $k^{-3/2}$ turbulence, where a is the wavevector-anisotropy constant $L_\parallel \approx a L_\perp$. The larger the value of a, the higher the Reynolds number. Using expression (31) for D_B, expression (36) for the turbulence Reynolds number (34) can be written as

$$R_{\text{turb-Bohm}} \;=\; 16\, a\, (u_o^{\,2}/v_A v_{Ti})\,(L_{\perp o}/r_{gi}) \qquad\qquad . \tag{37}$$

Evaluating expression (37) for Kraichnan $k^{-3/2}$ turbulence in the solar wind at 1 AU gives $R_{\text{turb-Bohm}} = a{\cdot}950$, for the Earth's magnetosheath it gives $R_{\text{turb-Bohm}} = a{\cdot}120$, and for the Earth's plasma sheet it gives $R_{\text{turb-Bohm}} = a{\cdot}5.1$. These values are entered into Table I.

VI. RATIOS OF SCALESIZES

In fully developed Navier-Stokes turbulence, the ratio of characteristic scalesizes in the turbulence is related to the turbulence Reynolds number (integral-scale Reynolds number) R_{turb}. For turbulence with spectral transfer progressing at the local eddy-turnover time, the ratio of the correlation length (large-eddy scale size) L_o to the Kolmogorov dissipation scale L_{Kol} is

$$L_o/L_{Kol} \sim R_{turb}^{3/4} \tag{38}$$

(cf. eq. (7.18) of Frisch[8]) and the ratio of the correlation length (large-eddy scale) L_o to the Taylor microscale L_{Tay} is

$$L_o/L_{Tay} \sim R_{turb}^{1/2} \tag{39}$$

(cf. eq. (3.2.17) of Tennekes and Lumley[1]). This is depicted in Figure 6.

For Kraichnan $k^{-3/2}$ turbulence with a constant kinematic shear viscosity ν and an energy cascade proceeding with $\tau_{weak} = v_A L_o^{1/2} L^{1/2} u_o^{-2}$ (expression (9)), the ratio of L_o to L_{Kol} can be calculated to be

$$L_o/L_{Kol} \sim R_{turb}^{2/3} \tag{40}$$

for Kraichnan $k^{-3/2}$ turbulence (with constant ν).

The well-known Reynolds-number scalings $L_o/L_{Kol} \sim R_{turb}^{3/4}$ and $L_o/L_{Tay} \sim R_{turb}^{1/2}$ (expressions (38) and (39)) are based on shear viscosity $\nu = $ constant, isotropic turbulence, and an energy transfer rate that goes at the local eddy-turnover time (giving the Kolmogorov $k^{-5/3}$ inertial-range energy spectrum). MHD turbulence in collisionless plasma may violate these assumptions. Taking the solar wind as an example, the energy spectrum of MHD turbulence may be $k^{-3/2}$ (Ref. 130) with a transfer rate weakened by the Alfven effect[84,88], the turbulence wavevector spectrum is anisotropic[131-133], and the functional form of the shear viscosity ν depends on the mechanism acting. And (see the following two paragraphs) the characteristic scalesizes of the plasma (the ion gyroradius and the ion skin depth) may interfere with the turbulence cascade.

A Navier-Stokes fluid has scale-invariant properties throughout the range of scalesizes at which turbulence operates: from the large-eddy scalesize to the Kolmogorov dissipation scale. The Navier-Stokes fluid ceases to be a fluid at scales comparable to and smaller than molecular mean-free path λ_{mfp}, but λ_{mfp} is always much smaller than the Kolmogorov scale L_{Kol}. This is shown as follows. The molecular kinematic viscosity ν of a fluid is $\nu \sim v_T \lambda_{mfp} = \lambda_{mfp}^2/\tau_{coll}$ (cf. eq. (765) of Jeans[82] or Sect. 6.2 of Chapman and Cowling[23]), where v_T is the molecular thermal

velocity and τ_{coll} is the molecular collision time. The Kolmogorov dissipation scale L_{Kol} is obtained by equating an eddy turnover time L/u with a viscous dissipation time L^2/ν, which yields $L_{Kol} = \nu/u_{Kol}$, with u_{Kol} being the fluctuation amplitude at the Kolmogorov dissipation scale L_{Kol}. Thus, the ratio of the Kolmogorov dissipation scale to the molecular mean-free path is

$$L_{Kol} / \lambda_{mfp} = v_T/u_{Kol} \qquad , \qquad (41)$$

the ratio of the molecular thermal speed to the turbulence fluctuation velocity at the Kolmogorov scale. Since $u_{Kol} < u_o$ and since the turbulent fluctuations are subsonic, $u_{Kol} < u_o \ll v_T$, expression (41) indicates that $L_{Kol} \gg \lambda_{mfp}$ always for turbulence in a Navier-Stokes fluid with collisional viscosity.

This is not necessarily the case for MHD turbulence in a collisionless plasma. MHD spatial scales are limited to scales larger than $L_{min} = max(r_{gi}, c/\omega_{pi})$, where r_{gi} is the thermal-ion gyroradius of the plasma and c/ω_{pi} is the ion skin depth (ion inertial length) of the plasma. Using $r_{gi} = (c/\omega_{pi}) \beta_i^{1/2} 2^{-1/2}$, this minimum scalesize for MHD L_{min} is conveniently written

$$L_{min} = c/\omega_{pi} \, max(2^{-1/2}\beta_i^{1/2} , 1) \qquad . \qquad (42)$$

(For the three plasmas being considered, the values of L_{min} are entered into Table I.) At scalesizes comparable to or smaller than L_{min}, MHD does not apply and the physics of turbulent spectral transfer probably differs from the spectral transfer in the MHD scales[134-138]. Plus plasma-kinetic processes become important at scalesizes near L_{min} (Refs. 100, 139, and 140). Thus, scale invariance in a plasma fails at L_{min}, or actually at scales a few times larger than L_{min}.

A. Dissipation from Landau Damping

When the dissipation (shear viscosity) in a collisionless plasma is due to Landau damping, the Kolmogorov scale can be larger than or smaller than L_{min}. In the next paragraph the Kolmogorov dissipation scale for Landau damping in a Kraichnan $k^{-3/2}$ cascade of turbulence is calculated; in the paragraph that follows that, the Kolmogorov dissipation scale for Landau damping in a Kolmogorov $k^{-5/3}$ cascade of turbulence is calculated.

The Kolmogorov dissipation scale L_{Kol} is the scalesize L where the dissipation timescale equals the spectral energy transfer timescale. Equating the spectral-transfer time for mildly anisotropic Kraichnan turbulence τ_{weak} as given by expression (9) with τ_{Landau} for mildly anisotropic turbulence as given by expression (23) and solving for L yields

$$L_{Kol-Landau} = (A/a^2)^{2/5} (v_A v_{Te}/u_o^2)^{2/5} (L_o^{1/2}c^2/\omega_{pe}^2)^{2/5} \qquad . \qquad (43)$$

The minimum spatial scale L_{min} where MHD is valid in a plasma is given by expression (42), using $\omega_{pi} = (m_e/m_i)^{1/2}\,\omega_{pe}$ expression (42) is written $L_{min} = (m_i/m_e)^{1/2}\,(c/\omega_{pe})\,\max(1,(\beta_i/2)^{1/2})$. Using this expression for L_{min} and expression (43) for $L_{Kol\text{-}Landau}$ to construct the ratio of $L_{Kol\text{-}Landau}$ to L_{min} yields

$$L_{Kol\text{-}Landau}/L_{min} \;=\; (A/a^2)^{2/5}\,(m_e/m_i)^{1/2}\,(v_A^{\,2}\,v_{Te}^{\,2}\,L_o\,\omega_{pe}\,/u_o^{\,4}\,c)^{1/5}\,/\,\max(1,(\beta_i/2)^{1/2}). \quad (44)$$

According to expression (44), it can be the case that the Kolmogorov dissipation scale for Landau damping is in the MHD range of scalesize. For the parameters of Table I expression (44) yields $L_{Kol\text{-}Landau} = 8.6\,a^{-4/5}\,L_{min}$ for the solar wind at 1 AU, $L_{Kol\text{-}Landau} = 4.0\,a^{-4/5}\,L_{min}$ for the Earth's magnetosheath, and $L_{Kol\text{-}Landau} = 4.2\,a^{-4/5}\,L_{min}$ for the Earth's plasma sheet. For all three of these plasmas with $a = 1$, the Kolmogorov dissipation scale for Landau damping in a $k^{-3/2}$ cascade is in the MHD range of scale sizes. However, it is likely that $a > 1$ (where $L_{\parallel} \approx a\,L_{\perp}$), so the Kolmogorov dissipation scale for mildly anisotropic Kraichnan turbulence may not be in the MHD range of scales.

In the Kolmogorov $k^{-5/3}$ turbulence, the spectral transfer of energy goes at the local eddy turnover time τ_{eddy}. To calculate the Kolmogorov scale, an eddy turnover time is equated to a dissipation time. Using expression (21) for the Landau-damping dissipation time (for reduced-MHD fluctuations below the critical-balance curve) and using $v_{Te} = (m_i/m_e)^{1/2}v_{Ti}$ (for $T_e = T_i$) and $\omega_{pe} = (m_i/m_e)^{1/2}\omega_{pi}$ yields

$$L_{Kol\text{-}Landau} \;=\; c/\omega_{pi}\,A^{1/2}\,2^{-1/2}\,(v_{ti}/v_A)^{1/2}\,(m_e/m_i)^{1/4} \qquad . \qquad (45)$$

The ratio v_{ti}/v_A can be written as $v_{ti}/v_A = 2^{-1/2}\beta_i^{\,1/2}$, so expression (45) becomes

$$L_{Kol\text{-}Landau} \;=\; c/\omega_{pi}\,A^{1/2}\,2^{-3/4}\,\beta_i^{\,1/4}\,(m_e/m_i)^{1/4} \qquad . \qquad (46)$$

The ratio of $L_{Kol\text{-}Landau}$ (expression (46)) to L_{min} (expression (42)) is thus

$$L_{Kol\text{-}Landau}/L_{min} \;=\; A^{1/2}\,2^{-3/4}\,\beta_i^{\,1/4}\,(m_e/m_i)^{1/4}\,/\,\max(2^{-1/2}\beta_i^{\,1/2},1) \qquad . \qquad (47)$$

In Figure 7, the ratio $L_{Kol\text{-}Landau}/L_{min}$ from expression (47) is plotted as a function of β_i for a hydrogen plasma ($m_i = 1836 m_e$) with $T_e = T_i$ (black curve); the value of A for expression (47) is parameterized from Figure 5. As can be seen in Figure 7, for all β_i values the Kolmogorov scale for Landau damping is smaller than L_{min}. In Figure 7 similar curves are plotted for a plasma with $T_e = 10\,T_i$ (blue) and $T_i = 10\,T_e$ (red). For those plasmas too, at all β_i values the Kolmogorov scale for Landau damping is smaller than L_{min}. For all cases at all β_i values, the "fabric" of the

plasma interferes with the cascade and the $k^{-5/3}$ MHD turbulence does not reach the Kolmogorov dissipation scale when Landau damping supplies the dissipation.

Note that for Landau damping, the Kolmogorov-turbulence Reynolds number scaling $L_o/L_{Kol} \propto R_{turb}^{3/4}$ (expression (38)) for Kolmogorov $k^{-5/3}$ turbulence and $L_o/L_{Kol} \propto R_{turb}^{2/3}$ (expression (40)) for Kraichnan turbulence do not hold. This is because, for Landau damping, the effective shear viscosity ν is not a constant (see Section IV). For Kolmogorov $k^{-5/3}$ turbulence, using expression (45) for the Kolmogorov scale $L_{Kol-Landau}$ (which assumes reduced-MHD) and using expression (29) for the turbulence Reynolds number $R_{turb-Landau}$ for Landau damping, it can algebraically be shown that

$$L_o/L_{Kol-Landau} = R_{turb-Landau}^{1/2} \qquad (48)$$

for Landau-damping dissipation of Kolmogorov turbulence rather than $R_{turb-Landau}^{3/4}$. For Kraichnan $k^{-3/2}$ turbulence, using expression (43) for the Kolmogorov scale $L_{Kol-Landau}$ (which assumes mildly anisotropic turbulence) and using expression (30) for the turbulence Reynolds number $R_{turb-Landau}$ for Landau damping, it can algebraically be shown that

$$L_o/L_{Kol-Landau} = R_{turb-Landau}^{2/5} \qquad (49)$$

for Landau-damping dissipation of Kraichnan turbulence rather than $R_{turb-Landau}^{2/3}$. Note that expression (49) is independent of the wavevector anisotropy a. The reader is reminded that, for Kraichnan turbulence, the turbulence Reynolds number is defined as $R_{turb} = \tau_{diss}/\tau_{spectral}$ instead of $R_{turb} = \tau_{diss}/\tau_{eddy}$.

B. Dissipation from Bohm Diffusion

When Bohm diffusion acts to produce the dissipation, the Kolmogorov dissipation scale is always much larger than the MHD minimum scale L_{min}.

For Kolmogorov $k^{-5/3}$ turbulence, equating an eddy turnover time L/u to the Bohm dissipation timescale L^2/D_B and using $u = u_o(L/L_o)^{1/3}$ yields the Kolmogorov scale $L_{Kol-Bohm} = D_B^{3/4} u_o^{-3/4} L_o^{1/4}$. With $D_B = ck_BT_i/16eB = r_{gi}v_{Ti}/16$ (expression (31) and using $r_{gi}/(c/\omega_{pi}) = 2^{-1/2} \beta_i^{1/2}$, the ratio of $L_{Kol-Bohm}$ to L_{min} (expression(42)) becomes

$$L_{Kol-Bohn}/L_{min} = 8^{-1} 2^{-3/8} \beta_i^{3/8} (v_{Ti}/u_o)^{3/4} (L_o/(c/\omega_{pi}))^{1/4} / max(2^{-1/2}\beta_i^{1/2},1) \qquad (50)$$

for Kolmogorov $k^{-5/3}$ turbulence. Because $v_{Ti} \gg u_o$ and $L_o \gg c/\omega_{pi}$, unless $\beta_i \to 0$, expression (50) indicates that $L_{Kol-Bohn}$ will be larger than L_{min}. In this case where Bohm diffusion supplies

the dissipation, a Kolmogorov dissipation scale of the turbulence will be in the MHD regime of spatial scales. And in this case the relation $L_o/L_{diss} = R_{turb}^{3/4}$ may hold.

For a Kraichnan $k^{-3/2}$ spectrum of turbulence, the Kolmogorov dissipation scale for Bohm diffusion is even larger (as can be seen by the curve crossing points in the various panels of Figure 3). This is because the cascade of energy is slowed in the Kraichnan cascade and so dissipation processes have more time to act on the turbulent fluctuations . Hence, for the Kraichnan $k^{-3/2}$ turbulence, the Kolmogorov dissipation scale $L_{Kol-Bohm}$ will also be within the range of MHD scale sizes of the plasmas.

VII. DISCUSSION: THE SOLAR WIND, THE MAGNETOSHEATH, AND THE EARTH'S PLASMA SHEET

The relative importance of Braginskii shear viscosity, Landau damping, and Bohm diffusion for MHD turbulence in the solar-wind, the Earth's magnetosheath, and the Earth's plasma sheet are assessed in the following three subsections using Figures 8-10. The curves plotted in Figures 8-10 are from the following expressions: τ_{Brag} (expression (16)), τ_{Bohm} (expression (33)), τ_{eddy} (expression (11)), τ_{weak} (expression (9)), τ_{Landau} in the top panels for reduced-MHD anisotropy (expression (22)), and τ_{Landau} in the bottom panels for mildly anisotropic turbulence (expression (23)). In all of the bottom panels, $a = 1$ is taken.

A. Turbulence in the Solar Wind at 1 AU

For the spatial scales pertaining to the inertial subrange of MHD turbulence in the solar-wind plasma at 1 AU, the timescales for the various processes are plotted in Figure 8 as a function of the eddy scalesize $L_\perp$. The top panel pertains to Kolmogorov $k^{-5/3}$ turbulence and the bottom panel pertains to Kraichnan $k^{-3/2}$ turbulence. In the top panel the Landau-damping curve assumes the turbulence is in the reduced-MHD regime below the critical-balance curve and in the bottom panel the Landau-damping curve assumes the turbulence is isotropic ($a = 1$).

As can be seen in the top panel of Figure 8, in the inertial subrange of Kolmogorov turbulence the dissipation timescales are $\tau_{Braginskii} > \tau_{Landau} > \tau_{Bohm}$. In the solar-wind plasma Landau damping provides 3 to 400 times as much shear viscosity as does Braginskii shear viscosity, depending on the eddy scalesize. For the MHD fluctuations of the solar wind, Braginskii shear viscosity is a minor perturbation compared with Landau damping. For the smaller eddies of the inertial subrange, the Landau-damping rate is within a factor of 10 of the Bohm-diffusion coefficient. As can be seen by comparing the blue and black curves and comparing the red and black curves in the bottom panel of Figure 8, a Kolmogorov dissipation scale could be reached in the MHD region of the solar-wind plasma if Bohm diffusion were acting to dissipate fluctuations, but a Kolmogorov scale within MHD cannot be reached with Landau-damping acting on Kolmogorov $k^{-5/3}$ turbulence.

As can be seen in the bottom panel of Figure 8, in the inertial subrange of Kraichnan turbulence the dissipation timescales are also $\tau_{Braginskii} > \tau_{Landau} > \tau_{Bohm}$ except at the smallest

spatial scales where the Landau-damping timescale becomes shorter than the Bohm timescale. Note that the spectral-transfer timescales are longer in the bottom panel (τ_{weak}) than in the top panel (τ_{eddy}) owing to the weakening of the eddy-eddy interactions by the Alfven effect in the Kraichnan turbulence. Comparing the blue and black curves in the bottom panel, it is clear that Landau damping can yield a Kolmogorov dissipation scale within the range of MHD scalesizes for isotropic Kraichnan $k^{-3/2}$ turbulence.

Note that the curves in the bottom panel of Figure 8 are drawn for $a = 1$, where $L_{\parallel} \approx a$ $L_{\perp}$. For $a > 1$ the τ_{weak} curve will be lowered (cf. expression (9)) and the τ_{Landau} curve will be raised (cf. expression (23)). In that case a Kolmogorov dissipation scale within the range of MHD scalesizes might not occur.

In Sections III, IV, and V turbulence Reynolds numbers for the solar wind at 1 AU were estimated (see Table I). The values for Landau damping providing the dissipation are $R_{turb-Landau}$ $= 1.1 \times 10^8$ for strongly anisotropic Kolmogorov $k^{-5/3}$ turbulence and $R_{turb-Landau} = a^2 \bullet 4.6 \times 10^5$ for mildly anisotropic Kraichnan $k^{-3/2}$ turbulence; the values for Bohm diffusion providing the dissipation are $R_{turb-Bohm} = 1.0 \times 10^4$ for strongly anisotropic Kolmogorov turbulence and $R_{turb-Bohm}$ $= a \bullet 950$ for mildly anisotropic Kraichnan turbulence; and the values for Braginskii shear viscosity providing the dissipation are $R_{turb-Bohm} = 1.0 \times 10^9$ for strongly anisotropic Kolmogorov turbulence and $R_{turb-Bohm} = a \bullet 1.8 \times 10^8$ for mildly anisotropic Kraichnan turbulence. For use as a gauge of these calculated Reynolds numbers, the only meaningful estimate of the turbulence Reynolds number of the solar wind is from Matthaeus et al.[141] and Weygand et al.[142]. Using years of spacecraft measurement, they obtained a value $R_{eff} = 260,000$ for the "effective" Reynolds number of the turbulence. This value lies between the calculated values of $R_{turb-Landau}$ and $R_{turb-Bohm}$. The value of R_{eff} was obtained from the ratio of the measured correlation length L_{corr} of the solar-wind magnetic field to the measured Taylor scale L_{Tay} (curvature of the correlation function at the origin) of the solar-wind magnetic field: $R_{eff} = (L_{corr}/L_{Tay})^2$, which is expression (39). As pointed out in Section VI, expression (39) is based on an assumption of Kolmogorov turbulence with the spectral energy transfer rate being $\tau_{eddy} = L_o/u_o$ (see pg. 65 of Tennekes and Lumley[1]), so $R_{eff} = (L_{corr}/L_{Tay})^2$ can only be implied to be R_{turb} if the turbulence has a Kolmogorov $k^{-5/3}$ energy spectrum. When the Alfven effect operates in the MHD turbulence, the expression may become $R_{eff} = (u_o/v_A)(L_{corr}/L_{Tay})^2$, which lowers the estimated

value of the turbulence Reynolds number for given measured values of L_o and L_{Tay}. The values used by Matthaeus et al.[141] and Weygand et al.[142] in the ratio were $L_{corr} = 1.2{\times}10^6$ km and $L_{Tay} = 2400$ km. It has been argued that the large-eddy spatial scale of MHD turbulence in the solar wind must be smaller than the non-evolving flux tubes which confine the solar-wind plasma and the turbulence (Bruno et al.[143,144] and Borovsky[145]). By measuring the distances between magnetic walls in the solar wind Borovsky[145] obtained a median value of $5.6{\times}10^5$ km (and a mean value of $1.4{\times}10^6$ km) for the transverse-to-$\underline{B}$ diameters of the magnetic flux tubes at 1 AU (see also Li[146]). This median size is entered into Table I as $L_{box_\perp}$. These flux-tube-diameter values agree with the transverse-to-flow correlation length of the solar-wind magnetic field obtained with two-spacecraft measurements: $5.1{\times}10^5$ km (Ref. 147) and $2.9{\times}10^5$ km (Ref. 148). Using the Vaezi et al.[149] measurements as an analogy, Borovsky[145] argued that the large-eddy size transverse to $\underline{B}$ will be about 1/4 of the size of the "box" containing the turbulence and took $L_o = 1.5{\times}10^5$ km as 1/4 of the diameter of a median-size flux tube (see Table I). If $L_o = 1.5{\times}10^5$ km were to be used in the numerator of the expression $R_{eff} = (L_{corr}/L_{Tay})^2$ with $L_{Tay} = 2400$ km in the denominator, then the value $R_{eff} = 3900$ would be obtained for the solar-wind turbulence. This value of 3900 is in the range of the calculated Bohm-diffusion values of the turbulence Reynolds number: $R_{turb-Bohm} = 1.0{\times}10^4$ for Kolmogorov turbulence and $R_{turb-Bohm} = 950$ for Kraichnan turbulence. Clearly, more values of L_o and more values of L_{Tay} need to be measured to make a proper assessment of the calculated R_{turb} numbers.

B. Turbulence in the Earth's Magnetosheath

For the spatial scales pertaining to the inertial subrange of MHD turbulence in the Earth's magnetosheath, the timescales for the various processes are plotted in Figure 9 as a function of the eddy scalesize $L_\perp$. The top panel pertains to strongly anisotropic Kolmogorov $k^{-5/3}$ turbulence and the bottom panel pertains to isotropic Kraichnan $k^{-3/2}$ turbulence with $a = 1$. In the top panel the Landau-damping curve assumes the turbulence is in the reduced-MHD regime below the critical-balance curve and in the bottom panel the Landau-damping curve assumes the turbulence is isotropic with $a = 1$.

As can be seen in the top panel of Figure 9, in the inertial subrange of Kolmogorov turbulence the dissipation timescales are $\tau_{Braginskii} > \tau_{Landau} > \tau_{Bohm}$. In the hot magnetosheath

plasma Landau damping provides 5 to 7 orders of magnitude more shear viscosity than does Braginskii shear viscosity, depending on the eddy scalesize. For the MHD fluctuations of the magnetosheath, Braginskii shear viscosity is irrelevant compared with Landau damping. For the magnetosheath Landau-damping dissipation is much closer to Bohm diffusion than it is to Braginskii shear viscosity. For the smaller eddies of the inertial subrange, the Landau-damping rate is within a factor of 8 of the Bohm-diffusion coefficient. As can be seen by comparing the blue and black curves and the red and black curves in the top panel of Figure 9, for Kolmogorov $k^{-5/3}$ turbulence a Kolmogorov scale could be reached in the MHD region of the magnetosheath plasma if Bohm diffusion were acting to dissipate fluctuations, but a Kolmogorov scale within MHD cannot be reached with Landau-damping acting.

As can be seen in the bottom panel of Figure 9, in the inertial subrange of Kraichnan turbulence the dissipation timescales are also $\tau_{Braginskii} > \tau_{Landau} > \tau_{Bohm}$ except at the smallest spatial scales where the Landau-damping timescale becomes shorter than the Bohm timescale. Note that the spectral-transfer timescales are longer in the bottom panel than in the top panel owing to the Alfven effect in the Kraichnan turbulence. Comparing the blue and black curves in the bottom panel, it is clear that a Kolmogorov dissipation scale within the range of MHD scalesizes is possible in the magnetosheath for the Kraichnan $k^{-3/2}$ turbulence.

C. Turbulence in the Earth's Magnetotail Plasma Sheet

For the spatial scales pertaining to the inertial subrange of MHD turbulence in the Earth's magnetotail plasma sheet, the timescales for the various processes are plotted in Figure 10 as a function of the eddy scalesize $L_\perp$. The top panel pertains to strongly anisotropic Kolmogorov $k^{-5/3}$ turbulence and the bottom panel pertains to isotropic Kraichnan $k^{-3/2}$ turbulence with $a = 1$. In the top panel the Landau-damping curve assumes the turbulence is in the reduced-MHD regime below the critical-balance curve and in the bottom panel the Landau-damping curve assumes the turbulence is isotropic.

This case is similar to the case of the magnetosheath discussed in Section VI.B. As can be seen in the top panel of Figure 10, in the inertial subrange of Kolmogorov turbulence the dissipation timescales are $\tau_{Braginskii} > \tau_{Landau} > \tau_{Bohm}$. In the very hot plasma-sheet plasma Landau damping provides 8.5 to 9.5 orders of magnitude more shear viscosity than does Braginskii shear viscosity. For the MHD fluctuations of the plasma sheet, Braginskii shear viscosity is irrelevant

compared with Landau damping. For the plasma sheet Landau-damping dissipation is much closer to Bohm diffusion than it is to Braginskii shear viscosity. For the smaller eddies of the inertial subrange of the plasma sheet, the Landau-damping rate is within a factor of 8 of the Bohm-diffusion coefficient. As can be seen by comparing the blue and black curves and the red and black curves in the top panel of Figure 10, for Kolmogorov $k^{-5/3}$ turbulence a Kolmogorov scale could be reached in the MHD region of the plasma-sheet plasma if Bohm diffusion were acting to dissipate fluctuations, but a Kolmogorov scale within MHD cannot be reached with Landau-damping acting.

As can be seen in the bottom panel of Figure 10, in the inertial subrange of isotropic (a=1) Kraichnan turbulence the dissipation timescales are also $\tau_{Braginskii} > \tau_{Landau} > \tau_{Bohm}$ except at the smallest spatial scales where the Landau-damping timescale becomes shorter than the Bohm timescale. Note again that the spectral-transfer timescales are longer in the bottom panel than in the top panel owing to the Alfven effect in the Kraichnan turbulence. Comparing the blue and black curves in the bottom panel, it is clear that a Kolmogorov dissipation scale within the range of MHD scalesizes is possible in the plasma sheet for the isotropic Kraichnan $k^{-3/2}$ turbulence. If the Kraichnan turbulence is anisotropic with $a > 1$, then the black "weak" curve in the bottom panel of Figure 10 is lowered and the blue "Landau" curve is raised: in that case the Kolmogorov dissipation scale may or may not be within the range of MHD scalesizes in the plasma sheet.

Note that the MHD turbulence of the plasma sheet has severe scalesize limitations. The box size transverse to $\underline{B}$ is about 6 R_E = 4×10^4 km (Ref. 150) and the minimum scalesize L_{min} for MHD to hold is about 700 km: this gives a dynamic range of MHD scalesizes of L_{box}/L_{min} = 55, which is less than two decades. Taking the ratio of the measured large-eddy size L_o = 1×10^4 km (Refs. 59 and 63) to L_{min} gives L_o/L_{min} = 14 for the scalesize range of the MHD turbulence in the plasma sheet. Being able to form an inertial subrange free from driving and dissipation seems unlikely. Perhaps that is why the measured frequency spectra of the MHD turbulence in the plasma sheet is anomalously steep[59,151]. In the parallel-to-$\underline{B}$ direction there are also limitations to the range of available MHD scalesizes. For turbulence measured 20 R_E downtail from the Earth and estimate of the maximum lengthscale parallel to $\underline{B}$ may be ~ 40 R_E = 2.5×10^5 km owing to the finite length of the plasma. This parallel scale restriction will not interfere with the critical-balance curve, which for $L_{\perp o}$ = 1×10^4 km (see Table I) requires $L_\parallel < (v_A/u_o)L_{\perp o}$ = 5.3×10^4 km.

VIII. SUMMARY

The Landau damping of shear Alfven waves provides a pathway to calculating a shear viscosity for a collisionless plasma.

For the various mechanisms that can operate in a collisionless magnetized plasma, the shear viscosities can be written in simple functional forms as a square of a lengthscale in the numerator and a timescale in the denominator. The kinematic shear viscosities due to Coulomb collisions ν_{Brag}, due to Bohm diffusion ν_{Bohm}, due to electron Landau damping $\nu_{Landau-e}$, and due to ion transit-time damping at the Landau resonance $\nu_{Landau-i}$ are:

$$\nu_{Brag} \sim r_{gi}^2/\tau_{ii} \tag{51a}$$

$$\nu_{Bohn} \sim r_{gi}^2/\tau_{ci} \tag{51b}$$

$$\nu_{Landau-e} \sim (c/\omega_{pe})^2/\tau_{transit-e} \tag{51c}$$

$$\nu_{Landau-i} \sim r_{gi}^2/\tau_{transit-i} \tag{51d}$$

(cf. expressions (15), (32), (25), and (26)). Expressions (51) indicate that Braginskii shear viscosity is equivalent to a random displacement of momentum by a thermal ion gyroradius r_{gi} every ion-ion Coulomb collision time τ_{ii}, Bohm diffusion is equivalent to a random displacement of momentum by a thermal ion gyroradius r_{gi} every ion cyclotron period τ_{ii}, electron Landau damping is equivalent to a random displacement of momentum by a electron skin depth c/ω_{pe} every thermal electron transit time in the disturbance $\tau_{transit-e}$, and ion-transit-time damping is equivalent to a random displacement of momentum by a thermal ion gyroradius r_{gi} every thermal ion transit time in the disturbance $\tau_{transit-e}$. Electron Landau damping dominates for $10^{-4} < \beta_e < 1$ and ion transit time damping dominates for $\beta_i > 1$.

Braginskii shear viscosity is a lower limit to the shear viscosity of a collisionless plasma, Bohm diffusion is an upper limit, and Landau damping provides a shear viscosity that is typically between the two values. Braginskii shear viscosity and Bohm diffusion have the functional forms of constant (scale-independent) shear viscosities as in Navier-Stokes. Landau damping has the functional form of a mild hyperviscosity; $\nu_{Landau} \propto k^{2/3}$ for Kolmogorov turbulence and $\nu_{Landau} \propto k^1$ for Kraichnan turbulence.

Integral-scale Reynolds numbers R_{turb} were constructed with the various mechanisms of shear viscosity using $R_{turb} = \tau_{diss}/\tau_{spectral}$ evaluated for large eddies, where $\tau_{spectral}$ is the spectral energy transfer timescale, which was taken to be τ_{eddy} for Kolmogorov $k^{-5/3}$ turbulence and τ_{weak}

$= (v_A/u_o) \tau_{eddy}$ for Kraichnan $k^{-3/2}$ turbulence. When Kolmogorov turbulence was considered, the turbulence was taken to be concentrated in the reduced-MHD regime below the critical balance curve in $k_\perp$-$k_\parallel$ space; when Kraichnan turbulence was considered, the turbulence was taken to be mildly anisotropic. For the MHD turbulence of the solar wind at 1 AU, Reynolds-number values R_{turb} in the range 1×10^3 to 2×10^9 are obtained for the various mechanisms supplying shear viscosity and for Kolmogorov and Kraichnan spectra. For dissipation by Landau damping, Reynolds numbers $R_{turb} \approx 1\times10^8$ and $R_{turb} \approx a^2 \cdot 5\times10^5$ are obtained for Kolmogorov and Kraichnan spectra in the solar wind, respectively, where a is a measure of the wavevector anisotropy of the Kraichnan turbulence. These values will vary with the varying parameters of the solar wind and the varying amplitudes of the solar-wind turbulence.

A preliminary estimate of the Reynolds number of the turbulence in the solar wind (based on estimates of the correlation length L_o and Taylor scale L_{Tay} of the turbulence and the assumption that the Reynolds-number scaling $L_o/L_{Tay} \sim R_{turb}^{1/2}$ holds for this turbulence) yields a value that is in best agreement with either (a) Landau damping in quasi-isotropic Kraichnan turbulence or (b) Bohm diffusion in Kolmogorov turbulence. The estimated turbulence Reynolds number indicates that Braginskii shear viscosity is insufficient.

The Kolmogorov dissipation scale may or may not be within the range of MHD spatial scales in a collisionless plasma, depending of the mechanism of dissipation and on whether the turbulence is strongly anisotropic Kolmogorov $k^{-5/3}$ or mildly anisotropic Kraichnan $k^{-3/2}$. For Kolmogorov turbulence with Landau damping supplying the dissipation, a Kolmogorov dissipation scale within MHD is not possible. For Kraichnan turbulence with Landau damping supplying the dissipation, the Kolmogorov dissipation scale can fall within MHD scales.

APPENDIX: EMPHASIZING PERPENDICULAR-TO-$\underline{B}$ VELOCITIES.

In this paper only the viscosity that acts on velocities that are perpendicular to the magnetic field is considered. For turbulence in collisionless plasmas, this appendix presents arguments and spacecraft data supporting the reasonableness of that notion.

There are two distinct types of anisotropy which can characterize turbulence: "wavevector anisotropy" and "variance anisotropy" (cf. Refs. 152 and 153). Wavevector anisotropy concerns the distribution of the directions of the gradients in the turbulence; variance anisotropy concerns the directional distribution of the fluctuation-magnetic-field vectors and the velocity vectors. It is the variance anisotropy which is considered here.

Theoretical arguments have been put forth that argue that the field and velocity fluctuations $\delta\underline{u}$ and $\delta\underline{B}$ in MHD turbulence should become aligned, with $\delta\underline{u}$ either parallel or antiparallel to $\delta\underline{B}$ (cf. Refs. 98, 154, 155). This is known as dynamic alignment, and it is exhibited in many simulations of MHD turbulence (e.g. Refs. 154, 156, 157). Solar-wind fluctuations also show a high degree of dynamic alignment.[158,159] Since, for incompressible turbulence and for weakly compressible turbulence, the fluctuating field $\delta\underline{B}$ is perpendicular to the mean field $\underline{B}_o$, dynamic alignment means that the turbulent-fluctuation velocities $\delta\underline{u}$ are also perpendicular to $\underline{B}_o$.

When examining the directions of the fluctuation velocities $\delta\underline{u}$ of MHD turbulence in comparison with the direction of the total (mean plus fluctuating) magnetic field $\underline{B}$, simulations of 3D MHD turbulence have shown that if parallel-to-$\underline{B}$ velocities are not initially present in the turbulence, then parallel-to-$\underline{B}$ velocities will not appear as the turbulence evolves.[160,161]

An examination in this appendix of the solar wind indicates that the velocity fluctuations $\delta\underline{u}$ are chiefly perpendicular to the magnetic field $\underline{B}$. Owing to the bulk motion of the solar wind and the Parker-spiral direction of the interplanetary magnetic field, in the frame of reference of a spacecraft there is a good deal of velocity $\underline{u}_{\parallel}$ parallel to $\underline{B}$ in the solar wind. Fully subtracting off the large bulk velocity of the solar wind is difficult since the bulk speed is not steady and the bulk-velocity vector is not purely radial (owing to interactions between solar-wind parcels (e.g. Refs. 162 and 163) and owing to the motions of magnetic flux tubes (e.g. Ref. 145)). Here we carry out a solar-wind analysis using 64-sec resolution measurements from the ACE spacecraft. In examining solar-wind measurements to discern the relative size of parallel-to-$\underline{B}$ velocities and perpendicular-to-$\underline{B}$ velocities in the MHD turbulence of the solar wind, the bulk solar wind

velocity is subtracted off in the following two different manners. (1) Tangential discontinuities are located in the solar-wind measurements and the solar wind is divided into parcels of plasma, one parcel between every two adjacent discontinuities. Then the mean velocity vector of each parcel is calculated and subtracted from the individual 64-sec-resolution velocity values within the parcel of plasma. (2) A running 65-minute average of the velocity vector is subtracted off of the 64-sec-resolution velocity values. Method (1) focuses the analysis on the MHD turbulence within the flux tubes of the solar wind. Method (2) allows field rotation and flow-velocity jumps from the solar-wind tangential discontinuities into the data analysis. (Note that the strong field rotation and strong flow shear across solar-wind tangential discontinuities are known to be highly Alfvenic.[164-166]) Subtracting the bulk flow $\underline{u}_o$ from the instantaneous total velocity u, the residual fluctuating velocity will be denoted $\underline{v}$ (i.e. $\underline{v} = \underline{u} - \underline{u}_o$). With the bulk solar-wind velocity vector subtracted off, the component $\underline{v}_{\|}$ of the velocity vector parallel to the instantaneous total magnetic field $\underline{B}$ and the component $\underline{v}_\perp$ perpendicular to $\underline{B}$ are calculated. The bulk-flow convection of the Parker-spiral mean field is subtracted off most accurately in the direction normal to the ecliptic plane, which in (r,t,n) coordinates is the normal (n) component.

In Figure 11 the distribution of the logarithm of the ratio of $v_{\perp n}/v_{\|n}$ with 64-sec time resolution is binned for the year 2001 using measurements from the ACE spacecraft. The blue curve is the distribution calculated by removing the solar-wind bulk flow velocity parcel-by-parcel with method (1) and the black curve in Figure 11 is the distribution calculated by removing the bulk speed with method (2). The red vertical dashed line in Figure 11 indicates the value where $v_{\|n}$ equals $v_{\perp n}$: binned values to the right of the dashed line have $v_{\|n} < v_{\perp n}$. The two distributions in Figure 11 are strongly skewed into the $v_{\|n} < v_{\perp n}$ region to the right of the dashed line. Hence, in the n-component direction where the solar-wind bulk flow is well subtracted, perpendicular-to-$\underline{B}$ fluctuating velocities in the solar-wind plasma dominate over parallel-to-$\underline{B}$ fluctuating velocities. As noted on the figure, the median value of the instantaneous ratio of $v_\perp/v_\|$ in the n direction is 3.4 using method (1) and the median value is 3.6 using method (2): for isotropically distributed vectors (dashed curve in Figure 11) the median value of $v_\perp/v_\|$ is expected to be $3^{1/2} = 1.73$.

Table I. Typical values of relevant parameters for the solar wind at 1 AU, for the Earth's magnetosheath, and for the Earth's magnetotail plasma sheet (cf. Refs. 59, 81, and 145). The factor a is the (unknown) wavevector anisotropy of the Kraichnan $k^{-3/2}$ turbulence.

	Solar wind	magnetosheath	Plasma sheet	
n $[cm^{-3}]$	6	25	0.3	number density
T_i [eV]	7	400	5000	ion temperature
T_e [eV]	15	70	700	electron temperature
B [nT]	6	25	10	magnetic field strength
β_i	0.47	6.4	6.0	ion beta
β_e	1.0	1.1	0.85	electron beta
r_{gi} [km]	45	80	700	ion gyroradius
c/ω_{pi} [km]	93	45	400	ion inertial length
v_A [km/s]	54	110	400	Alfven speed
v_{Ti} [km/s]	26	200	690	ion thermal speed
v_{Te} [km/s]	1600	3500	11,000	electron thermal speed
τ_{ii} [sec]	1.6×10^6	1.6×10^8	4.8×10^{11}	ion-ion Coulomb collision time
ν_{brag} $[cm^2/s]$	3.8×10^6	1.3×10^5	3.3×10^3	Braginskii shear viscosity
D_B $[cm^2/s]$	7.3×10^{11}	1.0×10^{13}	3.1×10^{14}	Bohm diffusion coefficient
u_o [km/s]	5	40	75	integral-scale velocity
L_{min} [km]	93	80	700	Minimum MHD scalesize
L_{box} [km]	6×10^5	3×10^4	4×10^4	plasma size transverse to $\underline{B}$
L_o [km]	1.5×10^5	8000	1×10^4	large eddy scalesize
L_{box}/L_{min}	6500	400	55	MHD dynamic range of plasma
τ_{eddy-o} [s]	2.1×10^4	200	130	integral-scale eddy turnover time
τ_{weak-o} [s]	$2.3\times10^5\,a^{-1}$	$550\,a^{-1}$	$690a^{-1}$	Integral-scale weak spectral time
A	3	80	70	Landau-damping A factor
$R_{turb-Brag}$	2.0×10^9	2.5×10^{10}	2.3×10^{12}	Kolmogorov-turbulence Reynolds number (Braginskii shear viscosity)
$R_{turb-Brag}$	$a\bullet1.8\times10^8$	$a\bullet9.0\times10^9$	$a\bullet4.3\times10^{11}$	Kraichnan-turbulence Reynolds number (Braginskii shear viscosity)
$R_{turb-Landau}$	1.1×10^8	4.4×10^4	1100	Kolmogorov-turbulence Reynolds number (Landau damping)
$R_{turb-Landau}$	$a^2\bullet4.6\times10^5$	$a^2\bullet2900$	$a^2\bullet19$	Kraichnan-turbulence Reynolds number (Landau damping)
$R_{turb-Bohm}$	1.0×10^4	330	25	Kolmogorov-turbulence Reynolds number (Bohm diffusion)
$R_{turb-Bohm}$	$a\bullet950$	$a\bullet120$	$a\bullet5.1$	Kraichnan-turbulence Reynolds number (Bohm diffusion)

Table II. Mechanisms that can dissipate MHD fluctuations in a plasma to act as a "viscosity". Note that the last source listed (plasma-wave diffusion) may be one of the mechanisms underlying Bohm diffusion.

SOURCE OF DISSIPATION	SCALESIZES INVOLVED	REFERENCE
Coulomb scattering	All scales	Section III
Landau damping	All scales	Section IV
Bohm diffusion	All scales	Section V
Cyclotron damping	Restricted to small scales $k_\parallel^{-1} \sim c/\omega_{pi}$	Refs. 100, 118, and 140
Line tying	All scales	Refs. 60, 167, and 168
Reconnection	Restricted to small scales $k_\perp^{-1} \sim c/\omega_{pi}$	Refs. 169 - 171
Plasma-wave diffusion	All scales	Refs. 172 - 174

References

[1]Tennekes, H., and J. L. Lumley, *A First Course in Turbulence* (MIT Press, Cambridge, 1972).

[2]Reynolds., O., Phil. Trans. Roy. Soc. Lond., 174, 935 (1883).

[3]Orszag, S. A., J. Fluid Mech., 50, 689 (1971).

[4]Novopashin, S., and A. Muriel, J. Exp. Theor. Phys., 95, 262 (2002).

[5]Ben-Dov, G., and J. Cohen, Phys. Rev. Lett., 98, 064503 (2007).

[6]Tritton, D. J., *Physical Fluid Dynamics* (Van Nostrand Reinhold, Cambridge, 1977), Ch. 19.

[7]Schlichting, *Boundary-Layer Theory* (McGraw-Hill, New York, 1979).

[8]Frisch, U., *Turbulence: The Legacy of A. N. Kolmogorov* (Cambridge University Press, Cambridge, 1995).

[9]Pope, S. B., *Turbulent Flows* (Cambridge University Press, New York, 2000).

[10]Kellogg, R. M., and S. Corrsin, J. Fluid Mech., 96, 641 (1980).

[11]Demetriades, A., P. J. Ortwerth, and W. M. Money, AIAA J., 19, 1091 (1981).

[12]Tong, C., and Z. Warhaft, Phys. Fluids, 6, 2165 (1994).

[13]Chew, G. G., M. L. Goldberger, and F. E. Low, Proc. Roy. Soc. Lond., A236, 112 (1956).

[14]Parker, E. N., Phys. Rev., 107, 924 (1957).

[15]Alfven, H. and C.-G. and Falthammar, *Cosmical Electrodynamics*, (Oxford University Press, London, 1963).

[16]Drell, S. D., H. M. Foley, and M. A. Ruderman, J. Geophys. Res., 70, 3131 (1965).

[17]Fejer, J. A., and K. F. Lee, J. Plasma Phys., 1, 387 (1967).

[18]Goertz, C. K., and R. W. Boswell, J. Geophys. Res., 84, 7239 (1979).

[19]Lamb, H., *Hydrodynamics*, 6th Ed. (Cambridge University Press, London, 1932), Sect. 326.

[20]Batchelor, G. K., *An Introduction to Fluid Dynamics* (Cambridge University Press, London, 1967) Sect. 1.6.

[21]Faber, T. E., *Fluid Dynamics for Physicists* (Cambridge University Press, Cambridge, 1995) Sect. 6.3.

[22]Braginskii, S. I., in *Reviews of Plasma Physics* (ed. M. A. Leontovich), (Consultants Bureau, New York, 1965) pg. 205.

[23]Chapman, S., and T. G. Cowling, *The Mathematical Theory of Non-Uniform Gases* (Cambridge University Press, London, 1953).

[24]Kaufman, A. N., Phys. Fluids, 3, 610 (1960).

[25]Landshoff, R., Phys. Rev., 76, 904 (1949).

[26]Piddington, J. H., Mon. Not. Royal Astron. Soc., 114, 651 (1954).

[27]Robinson, B. B., and I. B. Bernstein, Ann. Phys., 18, 110 (1962).

[28]Montgomery, D., J. Geophys. Res., 97, 4309 (1992).

[29]Piddington, J. H., *Cosmic Electrodynamics* (Wiley-Interscience, New York, 1969).

[30]Boyd, T. J. M., and J. J. Sanderson, *Plasma Dynamics* (Barnes and Noble, New York, 1969).

[31]Montgomery, D. C., and D. A. Tidman, *Plasma Kinetic Theory* (McGraw-Hill, New York, 1964).

[32]Cowling, T. G., *Magnetohydrodynamics* (Adam Hilger, Bristol, 1976).

[33]Chamberlain, J. W., Astrophys. J., 131, 47 (1960).

[34]Lemaire, J., and M. Scherer, Rev. Geophys. Space Phys., 11, 427 (1973).

[35]Heikkila, W. J., Astrophys. Space Sci., 23, 261 (1973).

[36]Paschmann, G., Plasma and particle observations at the magnetopause: implications for reconnection, in *Magnetic Reconnection in Space and Laboratory Plasmas* (ed. E. W. Hones), (American Geophysical Union, Washington, 1984) pg. 114.

[37]Thomsen, M. F., J. A. Stansberry, S. J. Bame, S. A. Fuselier, and J. T. Gosling, J. Geophys. Res., 92, 12127 (1987).

[38]Thomsen, M. F., J. T. Gosling, S. J. Bame, and T. G. Onsager, J. Geophys. Res., 95, 6363 (1990).

[39]Mann, G., H. Luhr, and W. Baumjohann, J. Geophys. Res., 99, 13315 (1994).

[40]Wilkinson, W. P., Planet. Space Sci., 51, 629 (2003).

[41]Lucek, E. A., T. S. Horbury, A. Balogh, I. Dandouras, and H. Reme, Ann. Geophys., 22, 2309 (2004).

[42]Ogilvie, K. W., J. T. Steinberg, R. J. Fitzenreiter, C. J. Owen, A. J. Lazarus, W. M. Farrell, and R. B. Torbert, Geophys. Res. Lett., 23, 1255 (1996).

[43]Farrell, W. M., A. C. Tribble, and J. T. Steinberg, J. Spacecr. Rockets, 39, 749 (2002).

[44]Friedman, H. W., and R. M. Patrick, Phys. Fluids, 14, 1889 (1971).

[45]Davis, H. A., M. A. Mahdavi, and R. H. Lovberg, J. Plasma Phys., 15, 293 (1976).

[46]Borovsky, J. E., M. B. Pongratz, R. A. Roussel-Dupre, and T.-H. Tan, Astrophys. J., 280, 802 (1984).

[47]Bosch, R. A., R. L. Berger, B. H. Failor, N. D. Delamater, G. Charatis, and R. L. Kauffman, Phys. Fluids B, 4, 979 (1992).

[48]Sojka, J. J., R. W. Schunk, J. F. E. Johnson, J. H. Waite, and C. R. Chappell, J. Geophys. Res., 88, 7895 (1983).

[49]Wilson, G. R., J. L. Horwitz, and J. Lin, Adv. Space Res., 13(4), 107 (1993).

[50]Lonngren, K., D. Montgomery, I. Alexeff, and W. D. Jones, Phys. Lett., 25A, 629 (1967).

[51]Alexeff, I., W. D. Jones, and K. Lonngren, Phys. Rev. Lett., 21, 878 (1968).

[52]Malmberg, J. H., C. B. Wharton, R. W. Gould, and T. M. O'Niel, 11, 1147 (1968).

[53]Wong, A. Y,, and D. R. Baker, Phys. Rev., 188, 326 (1969).

[54]Tu, C.-Y., and E. Marsch, Space Sci. Rev., 73, 1 (1995).

[55]Goldstein, M. L., D. A. Roberts, and W. H. Matthaeus, Ann. Rev. Astron. Astrophys., 33, 283 (1995).

[56]Bavassano, B., Space Sci. Rev., 78, 29 (1996).

[57]Bruno, R., Nuovo Cim. C, 20, 881 (1997).

[58]Oughton, S., Solar wind fluctuations: Waves and turbulence, in *Solar Wind Ten,* (ed. M. Velli, R. Bruno, and F. Malara), (American Institute of Physics, New York, 2003) pg. 421.

[59]Borovsky, J. E., R. C. Elphic, H. O. Funsten, and M. F. Thomsen, J. Plasma Phys., 57, 1 (1997).

[60]Borovsky, J. E., and H. O. Funsten, J. Geophys. Res., 108, 1284 (2003).

[61]Voros, Z., W. Baumjohann, R. Nakamura, A. Runov, M. Volwerk, T. L. Zhang, and A. Balogh, Phys. Plasmas, 11, 1333 (2004).

[62]Stepanova, M., T. Vucina-Parga, E. Antonova, I. Ovchinnikov, and Y. Yermolaev, J. Atmos. Solar Terr. Phys., 67, 1815 (2005).

[63]Weygand, J. M., M. G. Kivelson, K. K. Khurana, H. K. Schwarzl, S. M. Thompson, R. L. McPherron, A. Balogh, L. M. Kistler, M. L. Goldstein, J. Borovsky, and D. A. Roberts, J. Geophys. Res., 110, A01205 (2005).

[64]Sahraoui, F., G. Belmont, L. Rezeau, N. Cornilleau-Wehrlin, J. L. Pincon, and A. Balogh, Phys. Rev. Lett., 96, 075002 (2006).

[65]Zimbardo, G., Plasma Phys. Control. Fusion, 48, B295 (2006).

[66]Shevyrev, N. N., G. N. Zastenker, P. E. Eiges, and J. D. Richardson, Adv. Space Res., 37, 1516 (2006).

[67]Narita, Y., K.-H. Glassmeier, M. L. Goldstein, and R. A. Treumann, Cluster observations of shock-turbulenc interactions, in *Turbulence and Nonlinear Processes in Astrophysical Plasmas*, (ed. D. Shaikh and G. P. Zank), (American Institute of Physics, New York, 2007) pg. 215.

[68]Biskamp, D., *Magnetohydrodynamic Turbulence* (Cambridge University Press, New York, 2003).

[69]Marsch, E., and C.-Y. Tu, J. Geophys. Res., 95, 8211 (1990).

[70]Tessian, J. A., C. W. Smith, B. T. MacBride, W. H. Matthaeus, M. A. Forman, and J. E. Borovsky, Astrophys. J., 692, 684 (2009).

[71]Horbury, T. S., M. A. Forman, and S. Oughton, Plasma Phys. Control. Fusion, 47, B703 (2005).

[72]Podesta, J. J., Dependence of solar wind power spectra on the direction of the local mean magnetic field, submitted to Astrophys. J., 2009.

[73]Tu, C.-Y., and E. Marsch, J. Geophys. Res., 95, 4337 (1990).

[74]Verma, M. K., D. A. Roberts, M. L. Goldstein, S. Ghosh, and W. T. Stribling, J. Geophys. Res., 101, 21619 (1996).

[75]Pagel, C., and A. Balogh, Nonlinear Proc. Geophys., 8, 313 (2001).

[76]Veltri, P., Plasma Phys. Cont. Fusion, 41, A787 (1999).

[77]Podesta, J. J., D. A. Roberts, and M. L. Goldstein, J. Geophys. Res., 111, A10109 (2006).

[78]Vasquez, B. J., C. W. Smith, K. Hamilton, B. T. MacBride, and R. J. Leamon, J. Geophys. Res., 112, A07101 (2007).

[79]Chen, H., and D. Montgomery, Plasma Phys. Control. Fusion, 29, 205 (1987).

[80]Yoshizawa, A., and N. Yokoi, Phys. Plasmas, 3, 3604 (1996).

[81]Borovsky, J. E., Phys. Plasmas, 13, 056505 (2006).

[82]Jeans, J. H., *The Dynamical theory of Gases*, 4th ed. (Cambridge University Press, London, 1925).

[83]Montgomery, D., Theory of hydromagnetic turbulence, in *Solar Wind Five,* (ed. M. Neugebauer), (NASA Conference Publication 2280, NASA, Washington DC, 1983) pg. 107 .

[84]Matthaeus, W. H., and Y. Zhou, Phys. Fluids B, 1, 1029 (1989).

[85]Muller, C., and D. Biskamp, in *Lecture Notes in Physics 614*, (ed. E. Falgarone and T. Passot), (Springer-Verlag, Berlin, 2003) pg. 3.

[86]Verma, M. K., Phys. Reports., 401, 229 (2004).

[87]Iroshnikov, P. S., Sov. Astron., 7, 566 (1964).

[88]Kraichnan, R. H., Phys. Fluids, 8, 1385 (1965).

[89]Marsch, E., and C. Y. Tu, J. Geophys. Res., 98, 21045 (1993).

[90]Strauss, H. R., Phys. Fluids, 19, 134 (1976).

[91]Rosenbluth, M. N., D. A. Monticello, H. R. Strauss, and R. B. White, Phys. Fluids, 19, 1987 (1976).

[92]Kinney, R. M., and J. C. McWilliams, Phys. Rev. E., 57, 7111 (1998).

[93]Higdon, J. C., Astrophys. J., 285, 109 (1984).

[94]Goldreich, P., and S. Sridhar, Astrophys. J., 438, 763 (1995).

[95]Galtier, S., A. Pouquet, and A. Mangeney, Phys. Plasmas, 12, 092310 (2005).

[96]Shebalin, J. V., W. H. Matthaeus, and D. Montgomery, J. Plasma Phys., 29, 525 (1983).

[97]Montgomery, D., and W. H. Matthaeus, Astrophys. J., 447, 706 (1995).

[98]Dobrowolny, M., A. Mangeney, and P. Veltri, Phys. Rev. Lett., 45, 144 (1980).

[99]Zhou, Y., and W. H. Matthaeus, J. Geophys. Res., 95, 14881 (1990).

[100]Gary, S. P., and J. E. Borovsky, J. Geophys. Res., 109, A06105 (2004).

[101]Krall, N. A., and A. W. Trivelpiece, *Principles of Plasma Physics*, (McGraw-Hill, New York, 1973) Sect. 1.14.

[102]Braginskii, S. I., Soviet Phys. JETP, 6, 358 (1958).

[103]Simon, A., Phys. Rev., 100, 1557 (1955).

[104]Stepanov, K. N., Soviet Phys. JETP 34, 892 (1958).

[105]Fejer, J. A., and J. R. Kan, J. Plasma Phys., 3, 331 (1969).

[106]Stefant, R. J., Phys. Fluids, 13, 440 (1970).

[107]Hollweg, J. V., J. Geophys. Res., 104, 14811 (1999).

[108]Nicholson, D. R., *Introduction to Plasma Theory* (Wiley, New York, 1983).

[109]Gary, S. P., *Theory of Space Plasma Microinstabilities* (University Press, Cambridge, 1993).

[110]Tanaka, M., T. Sato, and A. Haegawa, Geophys. Res. Lett., 14, 868 (1987).

[111]Tanaka, M., and T. Sato, Phys. Fluids B, 1, 325 (1989).

[112]Geary, J. L., J.-N. Loboef, and T. Tajima, Phys. Fluids B, 2, 773 (1990).

[113]Gary, S. P., and K. Nishimura, J. Geophys. Res., 109, A02109 (2004).

[114]Gang, F., Phys. Fluids, B4, 3152 (1992).

[115]Gary, S. P., and J. E. Borovsky, J. Geophys. Res., 113, A12104 (2008).

[116]Passot, T., and A. Pouquet, J. Comp. Phys., 75, 300 (1988).

[117]Leveque, E., and Z. S. She, Phys. Rev. Lett., 75, 2690 (1995).

[118]Cranmer, S. R., and A. A. Ballegooijen, Astrophys. J., 594, 573 (2003).

[119]Bohm, D., E. H. S. Burhop, and H. S. W. Massey, in *The Characteristics of Electrical Discharges in Magnetic Fields*, (ed. A. Guthrie and R. K. Wakerling), (McGraw-Hill, New York, 1949) pg. 13.

[120]Rynn, N., Phys. Fluids, 7, 1084 (1964).

[121]Chen, F. F., *Introduction to Plasma Physics and Controlled Fusion*, 2nd Ed. (Plenum, New York, 1984).

[122]Lin, A. T., J. M. Dawson, and H. Okuda, Phys. Fluids, 23, 1316 (1980).

[123]Chu, C., M.-S. Chu, and T. Ohkawa, Phys. Rev. Lett., 41, 653 (1978).

[124]Taylor, J. B., and B. McNamara, Phys. Fluids, 14, 1492 (1971).

[125]Vahala, G., and D. Montgomery, J. Plasma Phys., 6, 425 (1971).

[126]Pecseli, H. L., and T. Mikkelsen, J. Plasma Phys., 34, 77 (1985).

[127]Biel, W., H. Kempkens, and J. Uhlenbusch, Plasma Phys. Control. Fusion, 40, 1845 (1998).

[128]Chen, F. F., Phys. Rev. Lett., 15, 381 (1965).

[129]Wakatani, M., and A. Hasegawa, Phys. Fluids, 27, 611 (1984).

[130]Podesta, J. J., D. A. Roberts, and M. L. Goldstein, Astrophys. J., 664, 543 (2007).

[131]Bavassano, B., M. Dobrowolny, G. Fanfoni, F. Mariani, and N. F. Ness, Solar Phys., 78, 373 (1982).

[132]Dasso, S., L. J. Milano, W. H. Matthaeus, and C. W. Smith, Astrophys. J., 635, L181 (2005).

[133]Sorriso-Valvo, L., V. Carbone, R. Bruno, and P. Veltri, Europhys. Lett., 75, 832 (2006).

[134]Leamon, R. J., C. W. Smith, N. F. Ness, W. H. Matthaeus, and H. K. Wong, J. Geophys. Res., 103, 4775 (1998).

[135]Biskamp, D., E. Schwarz, A. Zeiler, A. Celani, and J. F. Drake, Phys. Plasmas, 6, 751 (1999).

[136]Stawicki, O., S. P. Gary, and H. Lui, J. Geophys. Res., 106, 8273 (2001).

[137]Krishan, V., and S. M. Mahajan, J. Geophys. Res., 109, A11105 (2004).

[138]Gary, S. P., S. Saito, H. Li, Geophys. Res. Lett., 35, L02104 (2008).

[139]Gary, S. P., J. Geophys. Res., 104, 6759, (1999); Gary, S. P., J. Plasma Phys., 35, 431 (1986).

[140]Leamon, R. J., W. H. Matthaeus, C. W. Smith, and H. K. Wong, Astrophys. J., 507, L181 (1998).

[141]Matthaeus, W. H., S. Dasso, J. M. Weygand, L. J. Milano, C. W. Smith, and M. G. Kivelson, Phys. Rev. Lett., 95, 231101 (2005).

[142]Weygand, J. M., W. H. Matthaeus, S. Dasso, M. G. Kivelson, and R. J. Walker, J. Geophys. Res., 112, A10201 (2007).

[143]Bruno, R., V. Carbone, P. Veltri, E. Pietropaolo, and B. Bavassano, Planet. Space Sci., 49, 1201 (2001).

[144]Bruno, R., R. D'Amicis, B. Bavassano, V. Carbone, and L. Sorriso-Valvo, Planet. Space Sci., 55, 2233 (2007).

[145]Borovsky, J. E., J. Geophys. Res., 113, A08110 (2008).

[146]Li, G., in *Turbulence and Nonlinear Processes in Astrophysical Plasmas*, (ed. D. Shaik and G. P. Zank), (American Institute of Physics, New York, 2007), pg. 26.

[147]Chang, S. C., and A. Nishida, Astrophys. Space Sci., 23, 301 (1973).

[148]Richardson, J. D., and K. I. Paularena, J. Geophys. Res., 106, 239 (2001).

[149]Vaezi, V., E. S. Oh, and R. C. Aldredge, Exper. Thermal Fluid Sci., 15, 424 (1997).

[150]Birn, J., R. R. Sommer, and K. Schindler, J. Geophys. Res., 82, 147 (1977).

[151]Voros, Z., W. Baumjohann, R. Nakamura, M. Volwerk, A. Runov, T. L. Zhang, H. U. Eichelberger, R. Treumann, E. Georgescu, A. Balogh, B. Klecker, and H. Reme, J. Geophys. Res., 109, A11215 (2004).

[152]Smith, C. W., K. Hamilton, and B. J. Vasquez, in *Proceedings of Solar Wind 11 - SOHO 16* (European Space Agency, ESA SP-592, 2005), pg. 551.

[153]Smith, C. W., B. J. Valquez, and K. Hamilton, J. Geophys. Res., 111, A09111 (2006).

[154]Grappin, R., U. Frisch, J. Leorat, and A. Pouquet, Astron. Astrophys., 105, 6 (1982).

[155]Matthaeus, W. H., M. L. Goldstein, and D. C. Montgomery, Phys. Rev. Lett., 51, 1484 (1983).

[156]Ting, A. C., W. H. Matthaeus, and D. Montgomery, Phys. Fluids, 29, 3261 (1986).

[157]Matthaeus, W. H., A. Pouquet, P. D. Mininni, P. Dmitruk, and B. Breech, Phys. Rev. Lett., 100, 085003 (2008).

[158]Dobrowolny, M., A. Mangeney, and P. Veltri, Astron. Astrophys., 83, 26 (1980).

[159]Podesta, J. J., B. D. G. Chandran, A. Bhattacharjee, D. A. Roberts, and M. L. Goldstein, J. Geophys. Res., 114, A01107 (2009).

[160]Dmitruk, P., W. H. Matthaeus, and S. Oughton, Phys. Plasmas, 12, 112304 (2005).

[161]Pablo Dmitruk, private communication, 2009.

[162]Pizzo, V. J., J. Geophys. Res., 83, 5563 (1978).

[163]Riley, P., J. Atmos. Solar-Terr. Phys., 69, 32 (2007).

[164]Denskat, K. U., and L. F. Burlaga, J. Geophys. Res., 82, 2693 (1977).

[165]Neugebauer, M., J. Geophys. Res., 90, 6627 (1985).

[166]De Keyser, J., M. Roth, and A. Soding, Geophys. Res. Lett., 25, 2649 (1998).

[167]Borovsky, J. E., and J. Bonnell, J. Geophys. Res., 106, 28967 (2001).

[168]Borovsky, J. E., in *Multiscale Processes in the Earth's Magnetosphere: From Interball to Cluster*, (ed. J.-A. Sauvaud and Z. Nemecek), (Kluwer, Dordrecht, 2004) pg. 217.

[169]Carbone, V., P. Veltri, and A. Mangeney, *Phys. Fluids A, 2*, 1487 (1990).

[170]Matthaeus, W. H., P. Dmitruk, S. Oughton, and D. Mullan, in *Solar Wind Ten*, (ed. M. Velli, R. Bruno, and F. Malara), (American Institute of Physics, Washington DC, 2003) pg. 427.

[171]Dmitruk, P., and W. H. Matthaeus, *Phys. Plasmas, 13*, 42307 (2006).

[172]Tikhonchyk, V. T., and V. Y. Bychenkov, *J. Geophys. Res., 100*, 9535 (1995).

[173]Bruma, C., S. Cuperman, and K. Komoshvili, *Phys. Scripta, 72,* 224 (2005).

[174]Ishizawa, A., and N. Nakajima, *Nucl. Fusion, 47*, 1540 (2007).

[175]Borovsky, J. E., M. F. Thomsen, R. C. Elphic, T. E. Cayton, and D. J. McComas, *J. Geophys. Res., 103,* 20297 (1998).
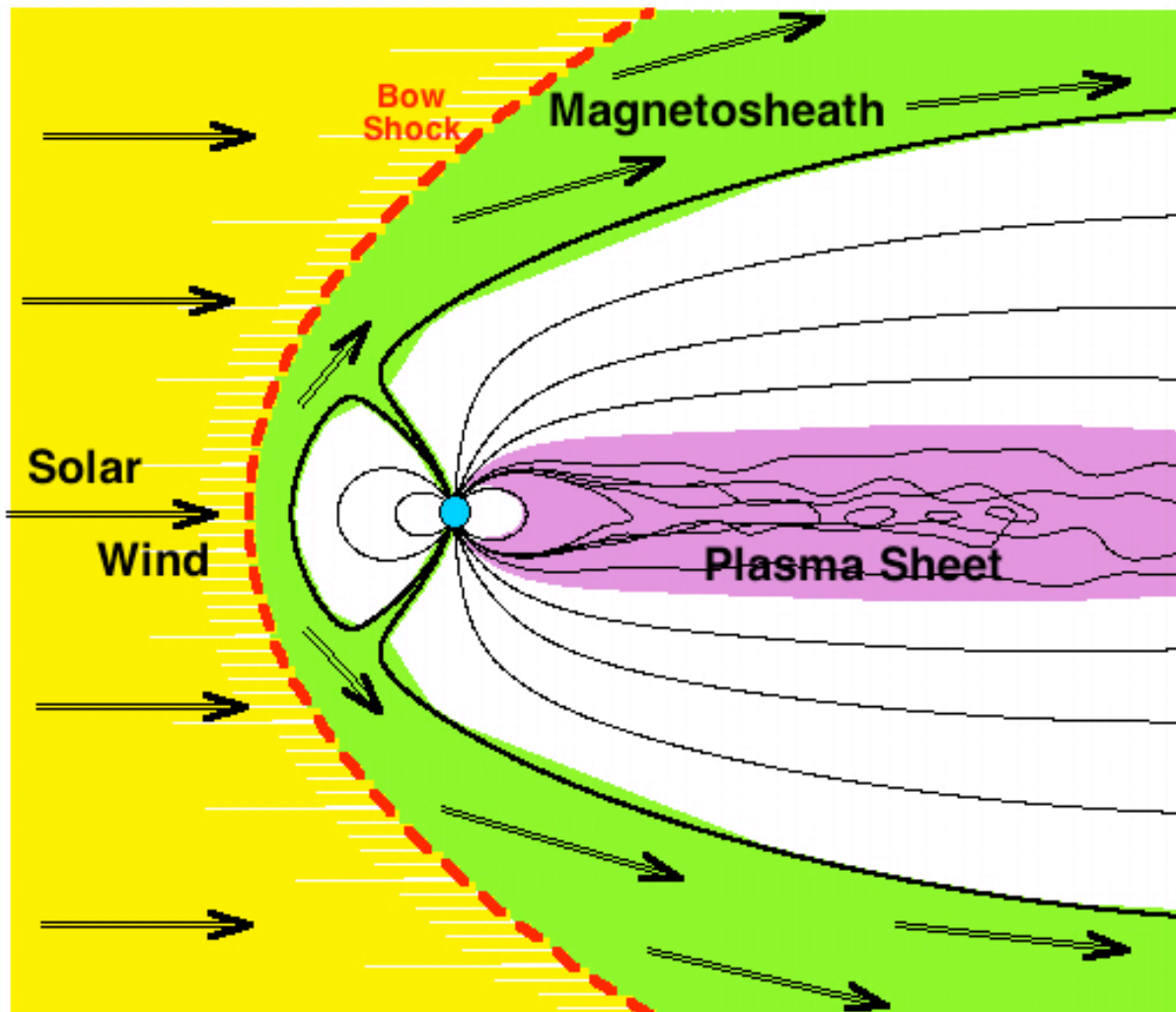
Figure 1. A sketch of the three collisionless magnetized plasmas studied herein that contain MHD turbulence: the solar wind, the magnetosheath, and the plasma sheet. The Earth is depicted as a blue sphere. The solar-wind plasma (shaded in yellow) impinges on the Earth's magnetic field from the right. Behind the bow shock (red dashed curve) the shocked solar-wind plasma flowing around the magnetosphere is known as the magnetosheath (shaded in green). The magnetosheath is denser, hotter, and has a stronger magnetic field than does the unshocked solar-wind plasma. Within the Earth's magnetotail is a very hot, low-density plasma known as the plasma sheet (shaded in purple). In the solar wind and the magnetosheath, no magnetic field lines are indicated. In the magnetosphere, magnetic-field lines are drawn in black by the method employed in Ref. 60. Note the large $\delta B/B_o$ in the turbulent plasma sheet.
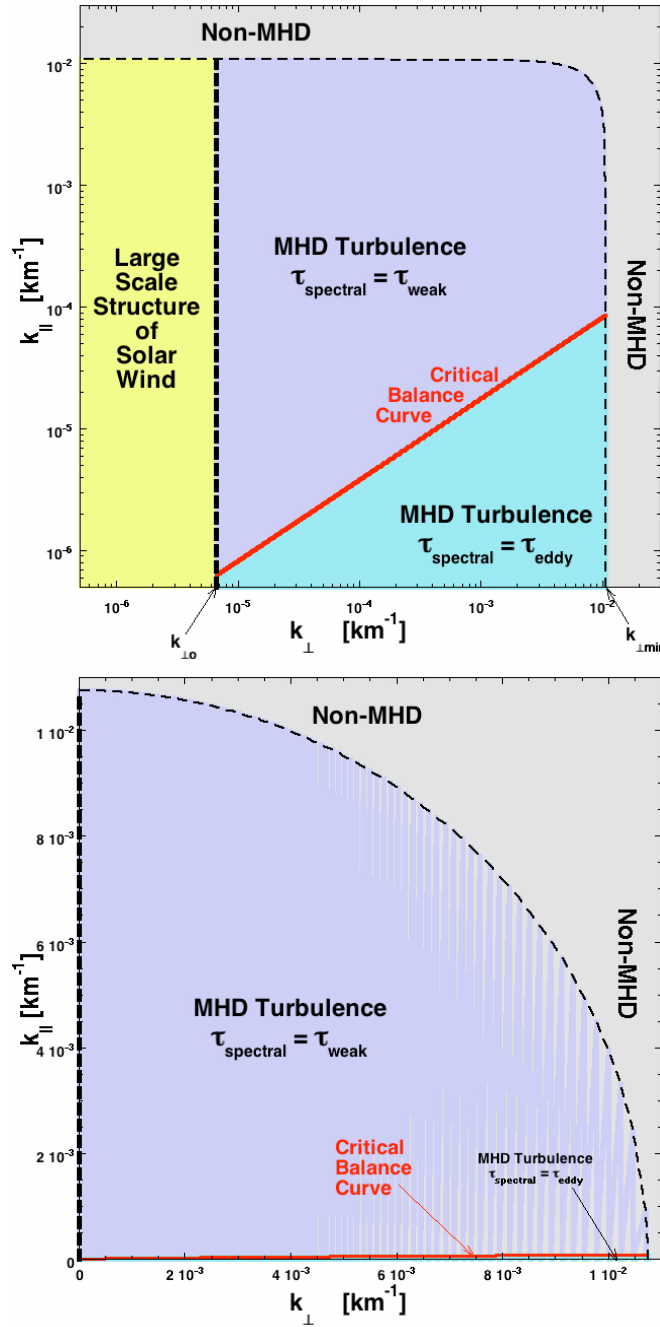
Figure 2. A sketch of the regimes of MHD turbulence in $k_\perp$-$k_\parallel$ space for the solar wind, where parallel and perpendicular are with respect to the direction of the magnetic field $\underline{B}$. Shaded in purple are regions where the Alfven effect is important and the Kraichnan $k^{-3/2}$ cascade should hold and shaded in blue are regions where the Alfven effect is negligible and the Kolmogorov $k^{-5/3}$ cascade should hold. The two regions are separated by the critical balance curve (red) where $\tau_{eddy} = \tau_A$. At perpendicular wavenumbers below the integral scale $k_{\perp o} = 1/L_o$ (thick black vertical dashed curve) the fluctuations are not part of the turbulence: this region is shaded in yellow. At wavenumbers larger than $k_{min} = 1/L_{min}$ (thin black dashed curve) the fluctuations are too small to be described by MHD: this region is shaded in gray. The top panel is a log-log plot, the bottom panel is a linear plot.
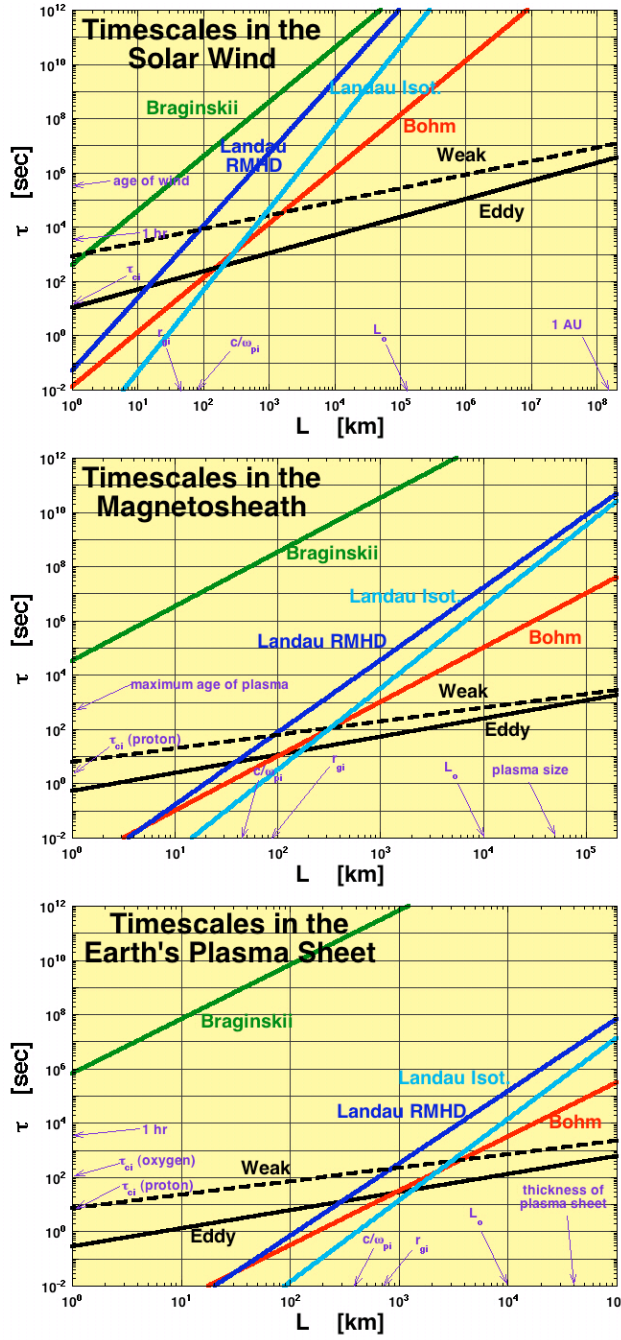
Figure 3. For the typical parameters in Table I, the timescales for turbulence in the solar wind at 1 AU (top panel), the Earth's magnetosheath (middle panel), and the Earth's plasma sheet (bottom panel) are plotted as functions of eddy size L. In all three panels the black solid curve is the eddy-turnover time for Kolmogorov $k^{-5/3}$ turbulence, the black dashed curve is the weakened spectral-transfer time for Kraichnan $k^{-3/2}$ turbulence, the green curve is the Braginskii viscous-dissipation timescale, the dark blue curve is the Landau-damping timescale for Kolmogorov $k^{-5/3}$ turbulence in the reduced-MHD regime, the light blue curve is the Landau-damping timescale for isotropic Kraichnan $k^{-3/2}$ turbulence, and the red curve is the Bohm-diffusion timescale. For the Kraichnan turbulence, $a = 1$ is taken for lack of better knowledge.
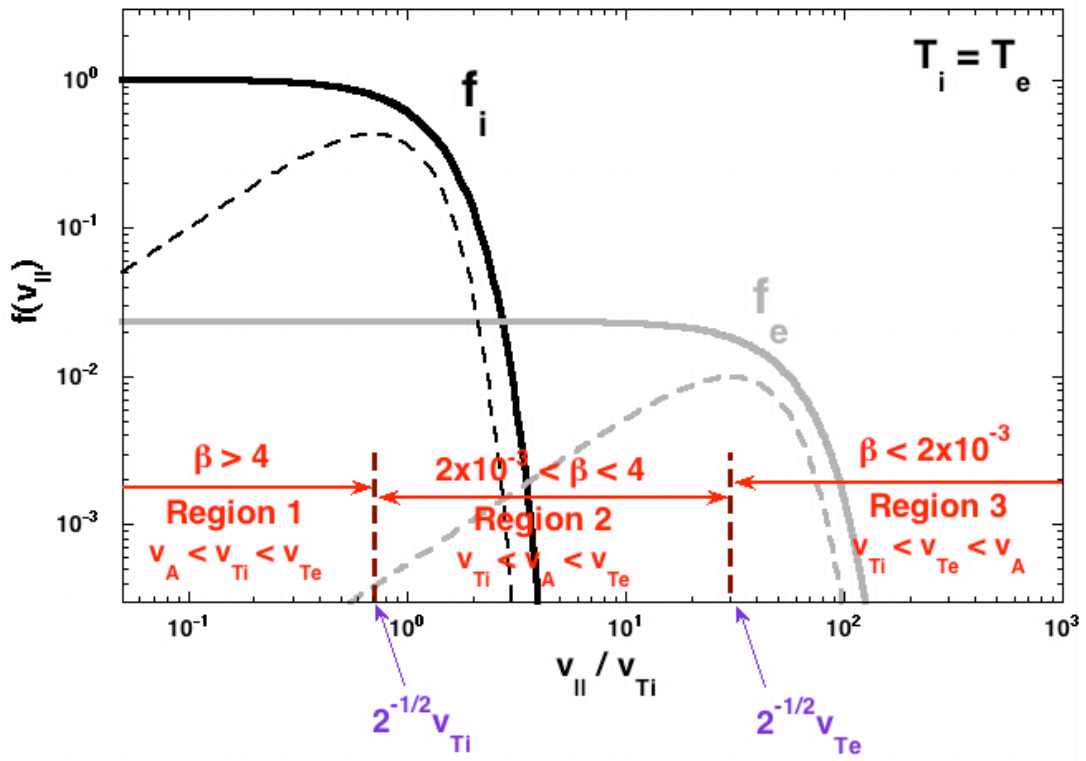
Figure 4. For a Maxwellian plasma with $T_i = T_e$, the ion distribution function $f_i(v_\parallel)$ is plotted (black solid curve) and the electron distribution function $f_e(v_\parallel)$ is plotted (gray solid curve) as function of $v_\parallel/v_{Ti}$. Also plotted as the dashed curves are $v_\parallel f_i(v_\parallel)$ for ions (black) and $v_\parallel f_e(v_\parallel)$ for electrons (gray). The position of the peaks of $v_\parallel f(v_\parallel)$ are marked as $v_\parallel = 2^{-1/2}v_{Ti}$ for ions and $v_\parallel = 2^{-1/2}v_{Te}$ for electrons.
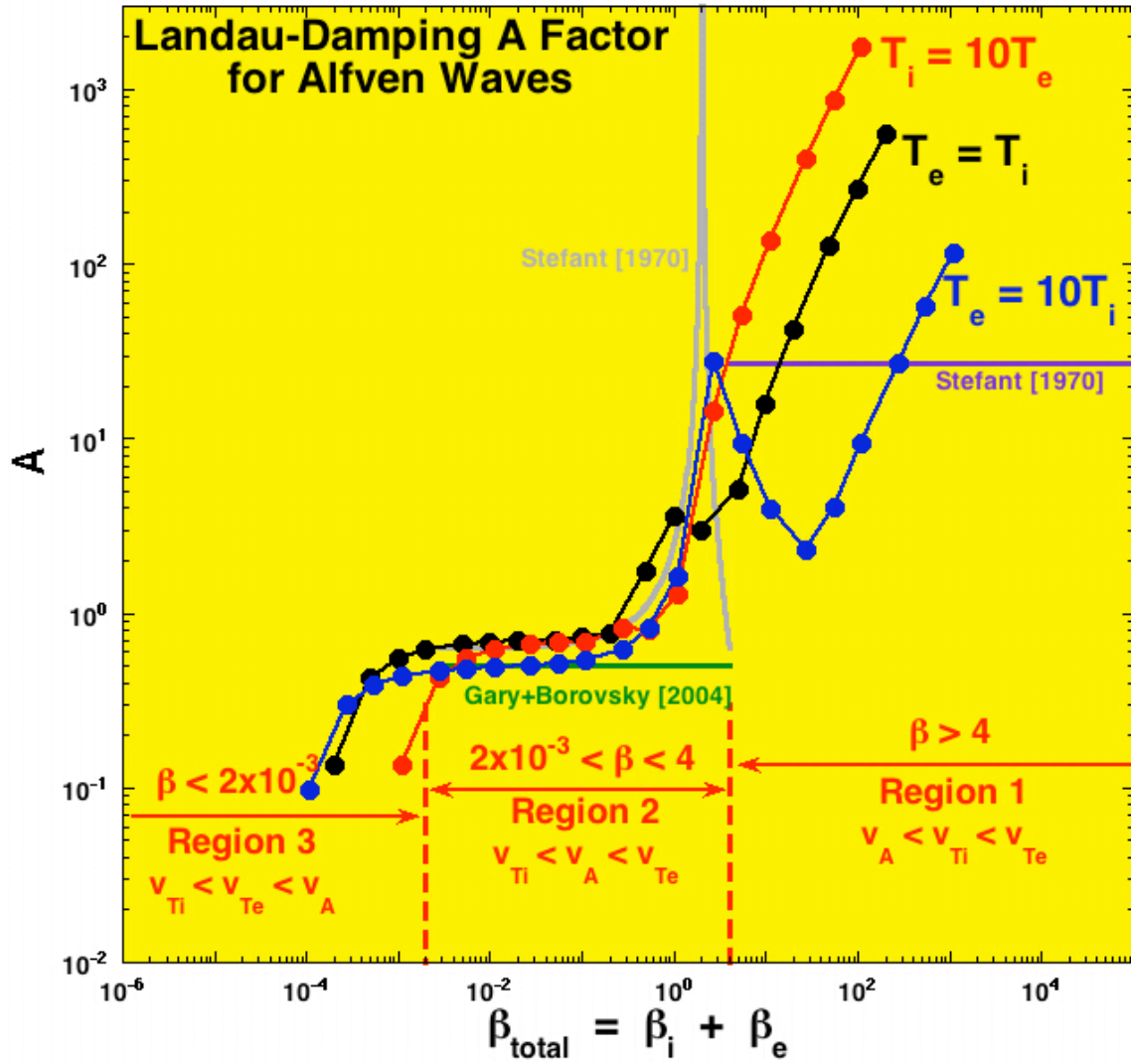
Figure 5. For a magnetized plasma with $T_e = T_i$ (black curve) and a plasma with $T_e = 10T_i$ (blue curve), the value of A in expression (19) is plotted as a function of $\beta_{total} = \beta_i + \beta_e$. The curves are determined from numerical solutions of the linear Vlasov-Maxwell equations for the Alfven-wave branch of the plasma dispersion relation. For comparison the value of A from Gary and Borovsky[100] (for $T_e \gg T_i$) is plotted in green, the value of A from expression (13b) of Stefant[106] is plotted in light blue, and the value of A from expression (19b) of Stefant[106] (for $T_e \gg T_i$) is plotted in purple. The regimes demarked by the red dashed lines apply to the $T_i = T_e$ case where $\beta_i = \beta_e = \beta_{total}/2$.
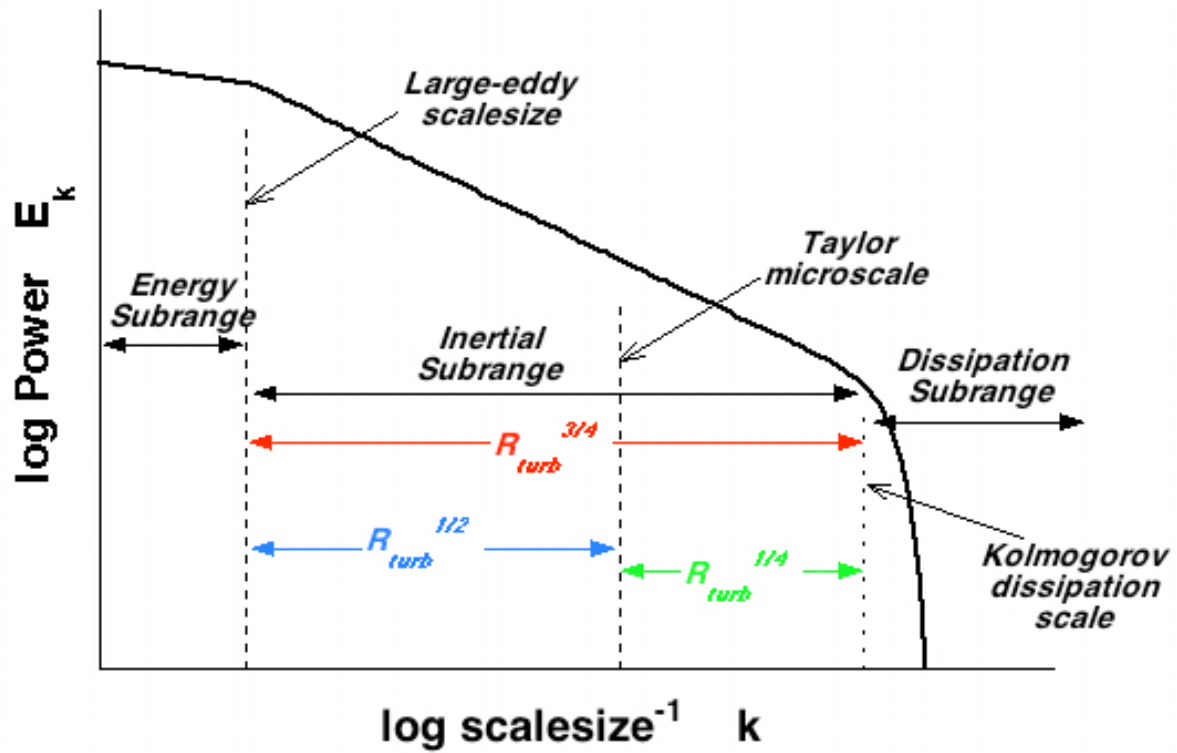
Figure 6. A sketch of the omnidirectional energy spectrum of Kolmogorov $k^{-5/3}$ turbulence with the three characteristic scale sizes (integral scale, Taylor scale, and Kolmogorov dissipation scale) and their relative values in relation to the turbulence Reynolds number R_{turb}. This scaling is only valid if the spectral energy transfer rate is proportional to the local-eddy turnover time.
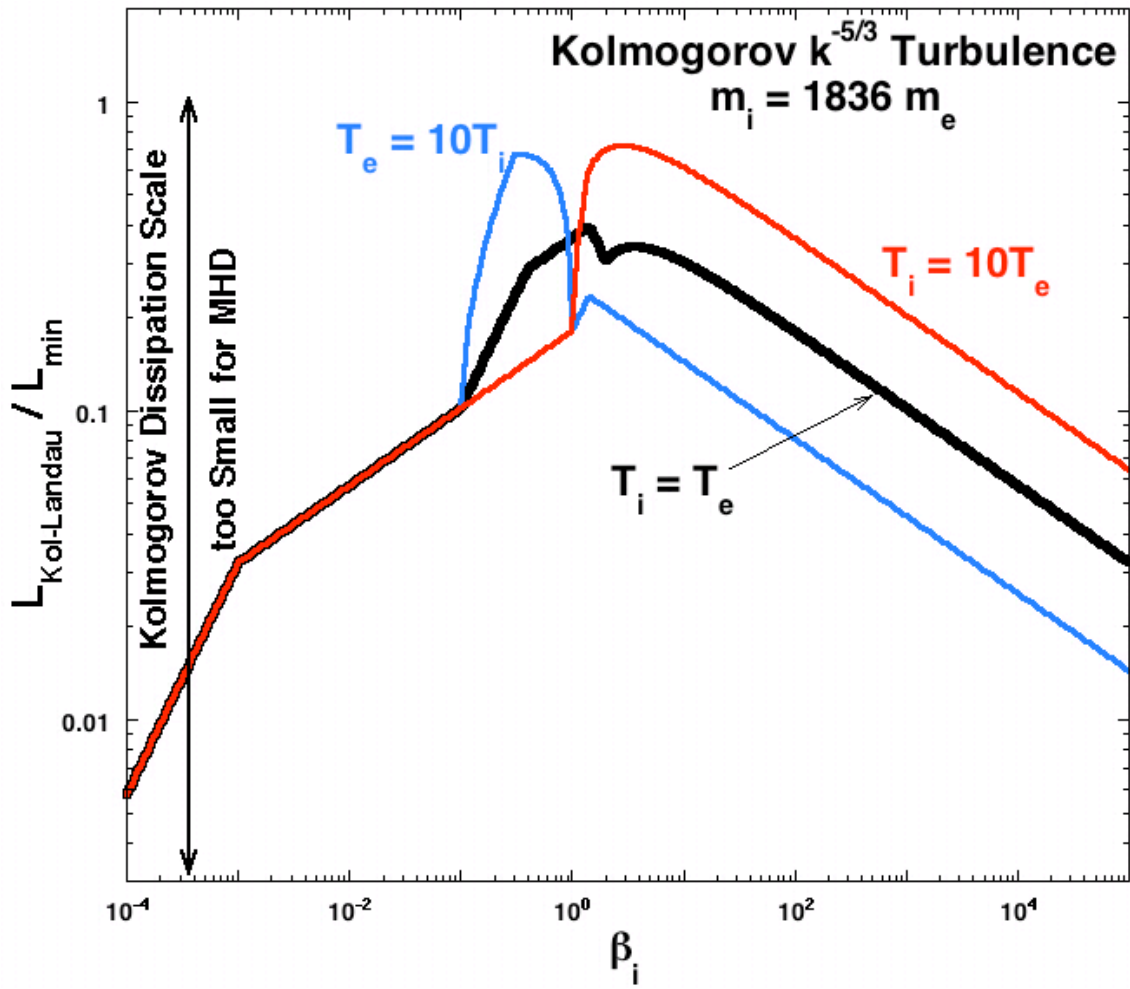
Figure 7. Using expression (47) with A obtained from Figure 5, the ratio of the Kolmogorov scale for Landau damping to the minimum-MHD scale of the plasma is plotted as a function of the ion beta of the plasma. Kolmogorov $k^{-5/3}$ turbulence in the reduced-MHD regime below the critical-balance curve is assumed in the calculations.
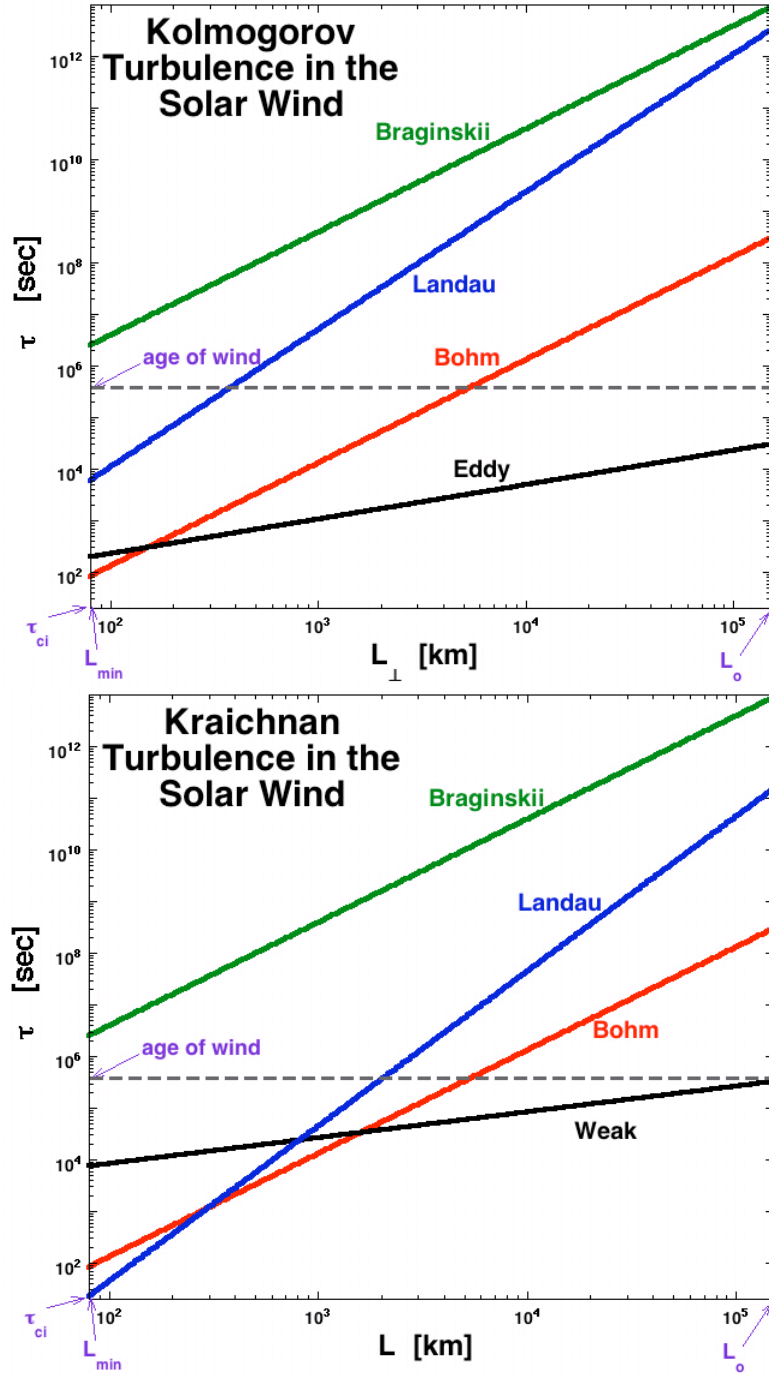
Figure 8. For Kolmogorov $k^{-5/3}$ turbulence (top panel) and Kraichnan $k^{-3/2}$ turbulence (bottom panel) in the solar wind at 1 AU, the timescales for eddy turnover (black), Bohm diffusion (red), Landau damping (blue), and Braginskii shear viscosity (green) are plotted. The horizontal axis extends from L_{min} of the solar wind to the large-eddy scalesize L_o. The vertical axis extends from the proton gyroperiod upward. The horizontal dashed line denotes the age of the solar-wind plasma at 1 AU (about 100 hours). All parameters come from Table I and $a = 1$ is taken.
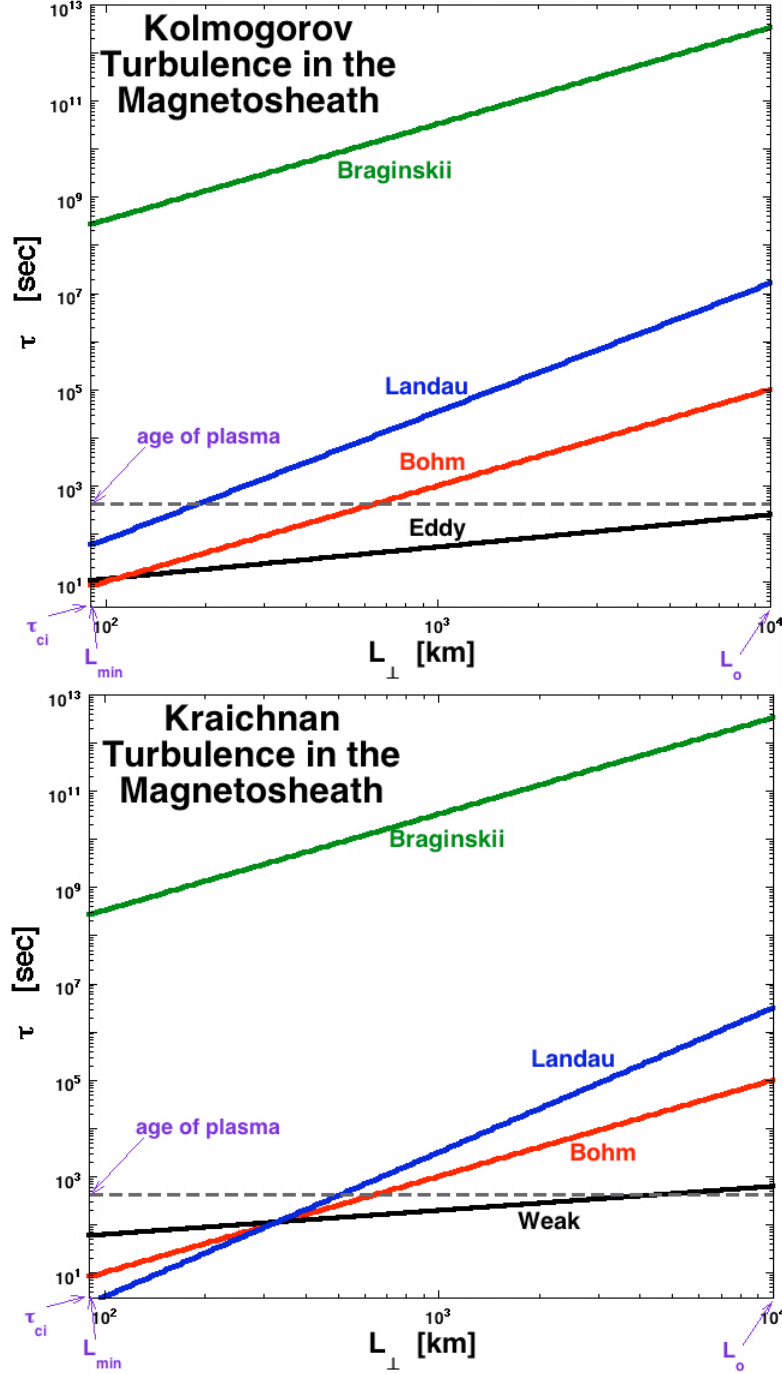
Figure 9. For Kolmogorov $k^{-5/3}$ turbulence (top panel) and Kraichnan $k^{-3/2}$ turbulence (bottom panel) in the Earth's magnetosheath, the timescales for eddy turnover (black), Bohm diffusion (red), Landau damping (blue), and Braginskii shear viscosity (green) are plotted. The horizontal axis extends from L_{min} of the magnetosheath plasma to the large-eddy scalesize L_o. The vertical axis extends from the proton gyroperiod upward. The horizontal dashed line denotes the approximate age of the magnetosheath plasma (about 500 seconds of flow time). All parameters come from Table I and a = 1 is taken.
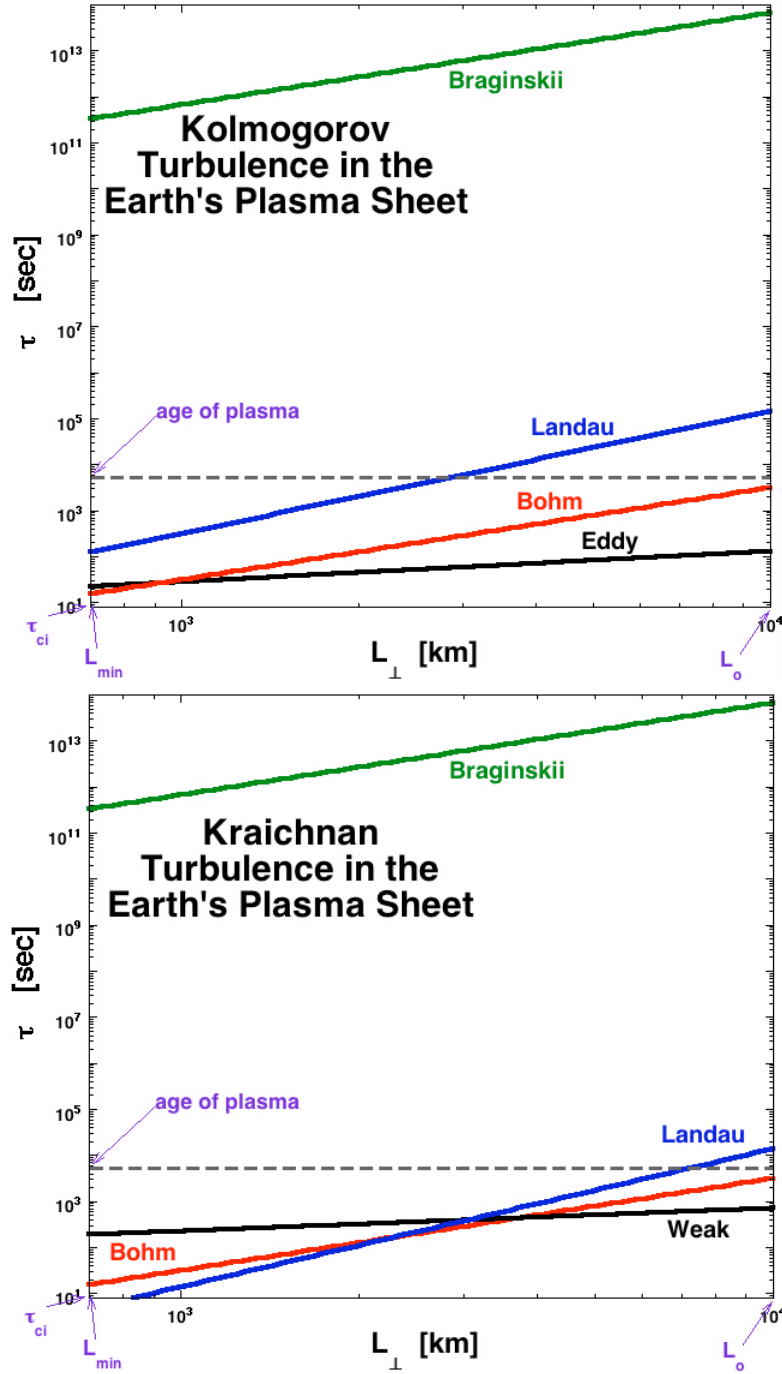
Figure 10. For Kolmogorov $k^{-5/3}$ turbulence (top panel) and Kraichnan $k^{-3/2}$ turbulence (bottom panel) in the Earth's magnetotail plasma sheet, the timescales for eddy turnover (black), Bohm diffusion (red), Landau damping (blue), and Braginskii shear viscosity (green) are plotted. The horizontal axis extends from L_{min} of the plasma sheet to the large-eddy scalesize L_o. The vertical axis extends from the proton gyroperiod upward. The horizontal dashed line denotes the approximate age of the plasma-sheet plasma (about 2 hours[175]). All parameters come from Table I and $a = 1$ is taken.
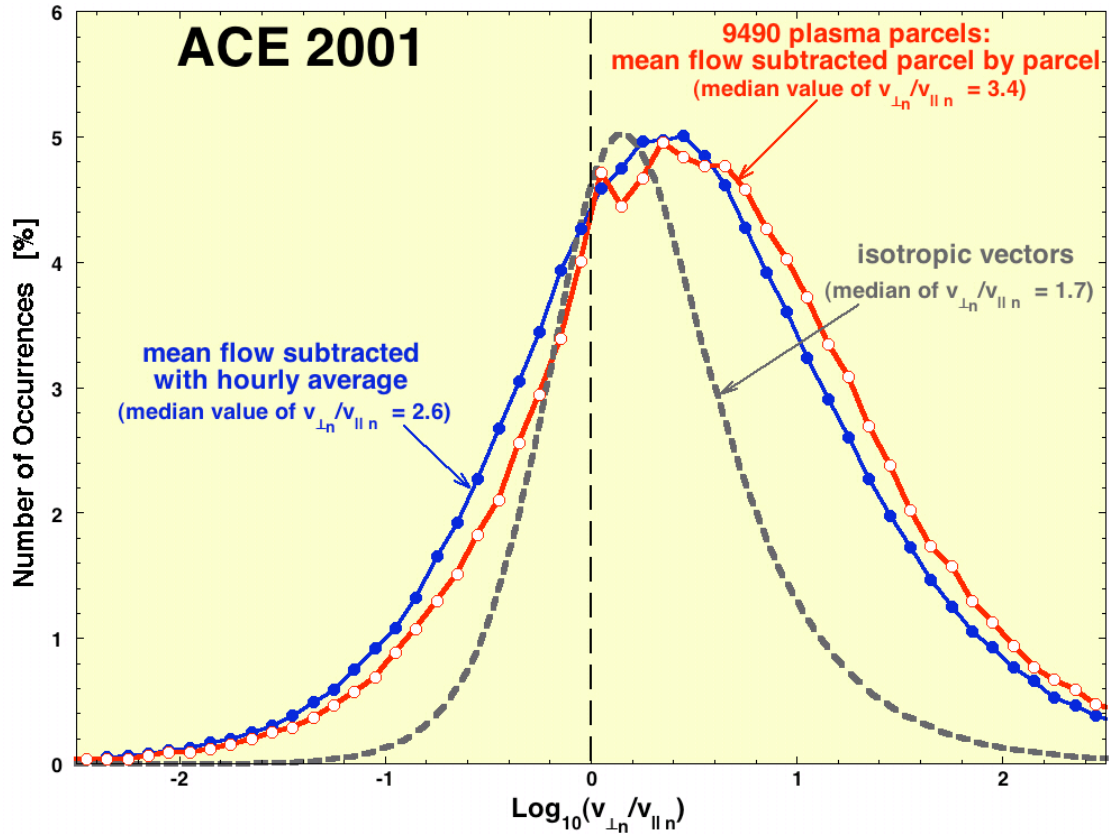
Figure 11. Using 64-sec time-resolution measurements of the solar-wind velocity from the ACE spacecraft for the year 2001, the logarithm of the ratio $v_{\perp n}/v_{\parallel n}$ of the solar-wind fluctuations is binned. To create the distribution plotted in red, the solar-wind bulk velocity is subtracted off the velocity measurement parcel by parcel (see text) and to create the distribution plotted in blue the solar-wind bulk velocity is subtracted off the measurements using a 65-minute running average. The dashed curve is the distribution of isotropically distributed vectors.